# The Mechanism of Energy Transfer in the Bacterial Photosynthetic Reaction Center

## Xanthipe J. Jordanides, Gregory D. Scholes,[†] and Graham R. Fleming*

*Department of Chemistry, University of California, Berkeley and Physical Biosciences Division, Lawrence Berkeley National Laboratory, Berkeley, California 94720*

*Received: September 29, 2000; In Final Form: December 5, 2000*

In the accompanying paper (Scholes, G. D.; Jordanides, X. J.; Fleming, G. R. *J. Phys. Chem.* **2001**, *105*, 1640), a generalization of Förster theory is developed to calculate electronic energy transfer (EET) in molecular aggregates. Here we apply the theory to wild-type and mutant photosynthetic reaction centers (RCs) from *Rb. sphaeroides*, as well as to the wild-type RC from *Rps. viridis*. Experimental information from the X-ray crystallographic structure, resonance Raman excitation profiles, and hole-burning measurements are integrated with calculated electronic couplings to model the EET dynamics within the RC complex. Optical absorption and circular dichroism spectra are calculated at various temperatures between 10 K and room temperature, and compare well with the experimentally observed spectra. The calculated rise time of the population of the lower exciton state of P, $P_-$, as a result of energy transfer from the accessory bacteriochlorophyll, B, to the special pair, P, in *Rb. sphaeroides* (*Rps. viridis*) wild-type at 298 K is 193 fs (239 fs), and is in satisfactory agreement with experimental results. Our calculations, which employ a weak-coupling mechanism suggest that the upper exciton state of P, $P_+$ plays a central role in trapping excitation from B. Our ability to predict the experimental rates is partly attributed to a proper calculation of the spectral overlap $J_{\delta\alpha}(\epsilon)$ using the vibronic progressions. The main advance we have made, however, is to calculate the electronic couplings $V_{\delta\alpha}$ in terms of the molecular composition of donor and/or acceptor aggregates, rather than treating the acceptors $P_+$ and $P_-$ as point dipoles associated with each spectroscopic band. Thus, we believe our electronic couplings capture the essence of the many-body interactions within the RC. Calculations for EET in two mutants, (M)-L214H (the beta mutant) and (M)H202L (the heterodimer), are in reasonable agreement with experimental results. In the case of the heterodimer the agreement depends on a decrease in the electronic couplings between $D_M$ and the rest of the pigments.

## I. Introduction

The photosynthetic reaction center (RC) of purple bacteria is a transmembrane pigment–protein complex present in the thylakoid membrane that efficiently accepts excitation energy from antenna complexes to initiate light-induced charge separation from the primary electron donor—the first step in photosynthesis. Figure 1 shows the arrangement of the pigments. The RC consists of three protein subunits: L, M, and H. The L and M subunits have relative 2-fold symmetry between them, and consist of five transmembrane helices that bind 10 cofactors: two closely spaced bacteriochlorophyll-*a* molecules ($P_L$ and $P_M$) that comprise the so-called "special pair", two monomeric "accessory" bacteriochlorophyll-*a* molecules ($B_L$ and $B_M$), two bacteriopheophytins ($H_L$ and $H_M$), two ubiquinones ($Q_A$ and $Q_B$), a carotenoid (Car), and a non-heme iron, as depicted in Figure 1.[1,2] Because of the strong coupling within the molecular dimer $P_L P_M$, the excited state is split into states that are symmetric (+) and antisymmetric (−) linear combinations of $P_L^* P_M$ and $P_L P_M^*$, which for the special pair are denoted as the exciton states $P_+$ and $P_-$. According to the protein subunits that bind the cofactors, these branches are denoted L and M, whereas in the nomenclature of the cofactors, one branch is denoted the A (active, electron transfer) branch and the other the B branch.[3]

The determination of the three-dimensional crystal structures of the RC, first of the species *Rhodopseudomonas* (*Rps.*) *viridis*[4,5] and later of *Rhodobacter* (*Rb.*) *sphaeroides*,[1,6] provided the impetus for the development of a molecular level description of the mechanism of light-induced electron and energy transfer.

As early as 1972 Slooten, using absorption measurements, proposed that electronic energy transfer (EET) from H and B to P occurs in the *Rb. sphaeroides* RC.[7] In 1986 such energy transfer was shown to occur from B to P for the RC of *Rps. viridis* in less than 100 fs at 298 K.[8] Two years later, Breton et al. demonstrated a similar result at 10 K for the same species.[9] Within the time resolution of these experiments, the energy transfer time was insensitive to temperature. Many other workers later reported a similar ultrafast energy transfer from B to P at room temperature for *Rb. sphaeroides*.[10–20] Using transient absorption, Jia et al. resolved an energy transfer time of 116 fs from B to P.[10] Later, Jonas et al. used pump–probe anisotropy to ascribe 80 and 150 fs components to B to P energy transfer and $P_+$ to $P_-$ internal conversion, respectively.[12] Multicolor transient absorption measurements performed by Vos et al., possibly the most detailed study of ultrafast energy transfer and internal conversion in the RC, reveal that internal conversion from the upper to lower exciton states of P is faster than energy transfer.[16] In addition, they reported energy transfer times in *Rps. viridis* of ≈ 90 fs at 298 K and ≈ 80 fs at 15 K and in *Rb. sphaeroides* of ≈ 180 fs at both 298 and 15 K.[16] Several other groups have reported similar results.[15,17–19] A temperature dependent study of *Rb. sphaeroides*, performed by Boxer and

---

\* Corresponding author. E-mail: GRFleming@lbl.gov. FAX: 510-642-6340.

† Present address: Lash Miller Chemical Laboratories, 80 St. George Street, University of Toronto, Toronto, Ontario, Canada M5S 3H6.
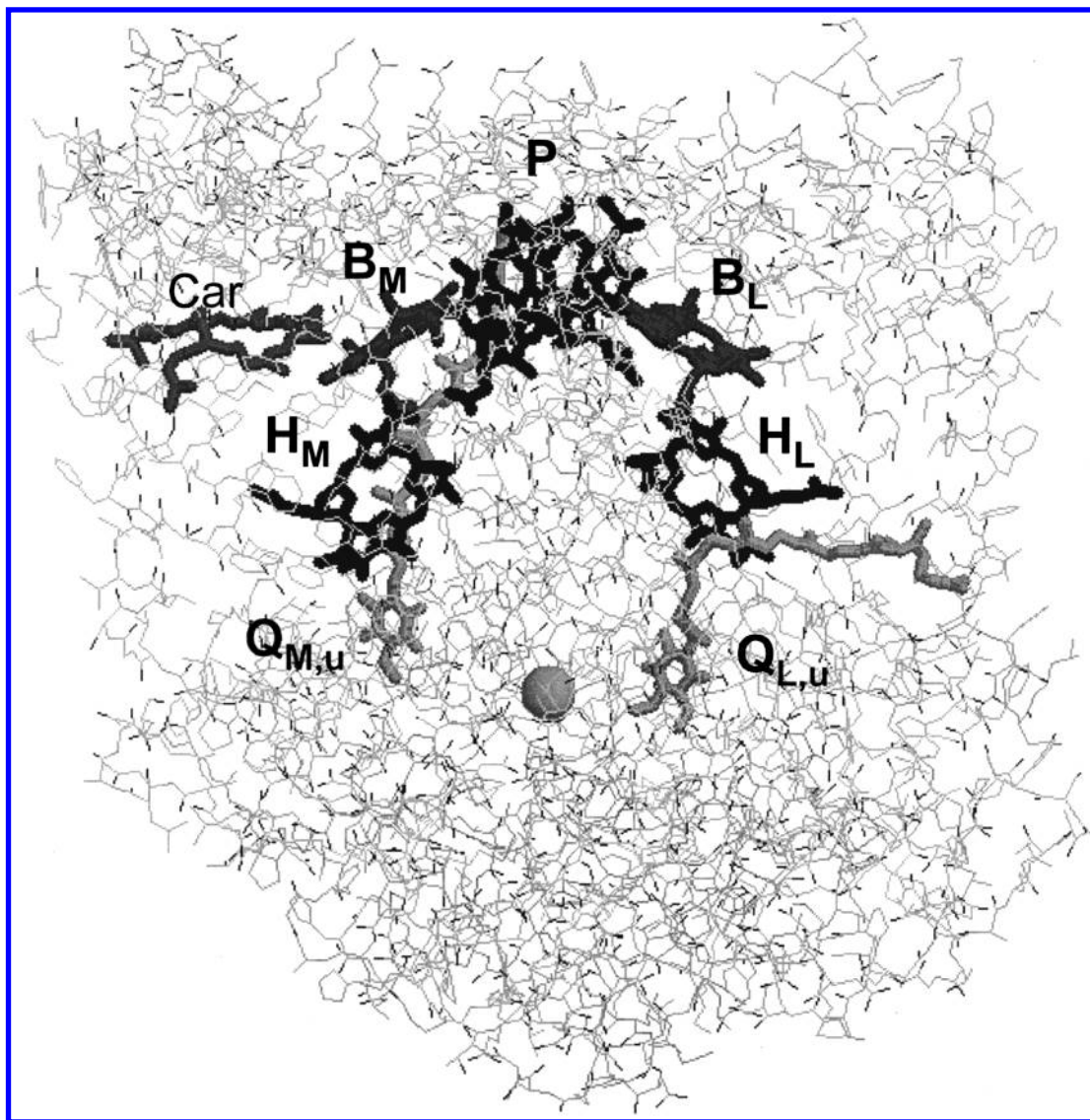
**Figure 1.** Schematic of the three-dimensional crystal structure of the RC for *Rb. sphaeroides*,[6] which has three protein subunits, L, M, and H. The arrangement of the RC cofactors are shown in wireframe: P is the special pair electron donor; B is the monomeric bacteriochlorophyll *a*; H is the monomeric bacteriopheophytin *a*; Q is the ubiquinone and Car is a carotenoid molecule. Here, following the authors of refs 1 and 2, the subscripts L or M denote the protein subunit associated with each cofactor.

co-workers using fluorescence up-conversion, resolved energy transfer times of 121 and 163 fs at 200 and 85 K, respectively,[13] indicating a weak temperature dependence of energy transfer from B to P. In addition, the appearance of P following excitation of H was shown to be ∼50% slower than that from direct excitation of B, and it was suggested that B was involved as a real intermediate.[13] The ultrafast time scales, yet apparent modest donor−acceptor spectral overlap has prompted numerous discussions concerning the mechanism of the energy transfer.

An initial attempt to calculate the energy transfer rate for *Rps. viridis* used a Pauli master equation calculation (using Förster theory) to obtain time-dependent populations.[21] The time constant for room-temperature EET from B to the lowest exciton state of P was calculated to be ≈3 ps.[21] On the other hand, times comparable to experimental values (∼150 fs) were predicted by employing a set of delocalized states in a Förster-type calculation at room temperature.[15] Haran et al. suggested that the very broad absorption band of P− centered at 860 nm for *Rb. sphaeroides* overlaps significantly with the accessory BChl$_a$ emission spectrum, thus the EET mechanism would be dominated by interactions between B and P−.[15] However, if the Förster mechanism for EET is applicable and is dominated by

spectral overlap between B and P−, it is thought that the rate of low-temperature energy transfer should be much slower than at room-temperature owing to the large (25 nm) spectral red-shift of the lower exciton state, P− at 10 K. Thus, it was later suggested that the Förster mechanism is unlikely to mediate the EET at any temperature.[13] Several groups proposed alternative mechanisms. For example, Jean et al. suggested that a Förster dipole−dipole mechanism could not explain EET in the RC and proposed that electronic couplings are possibly enhanced by orbital overlap dependent contributions.[21] Boxer and co-workers also suggested the importance of direct orbital overlap by comparing results from wild-type and from a heterodimer mutant.[17] Woodbury and co-workers suggested that the B to P energy transfer may be limited by nuclear motion and not by electronic coupling.[14] Others also argued, but without extensive modeling, that a strong coupling mechanism is likely to be required for a description of energy transfer from B to P.[11,12,16] Doubt was expressed that a modified version of Förster theory could account for these remarkably fast EET times.[22] Recently, Sumi suggested that the failure of Förster theory originates because of a breakdown in the description of the EET process in terms of the pairwise rates.[23] We came to a similar conclusion

**TABLE 1: Transition Dipole Unit Vectors (*x,y,z*) for the Q$_y$ Transitions of *Rb. sphaeroides*[a]**

|       | $\mu_x$  | $\mu_y$   | $\mu_z$  |
|-------|----------|-----------|----------|
| P$_M$ | 0.8546   | 0.5051    | 0.1206   |
| P$_L$ | −0.9649  | −0.02504  | 0.2613   |
| B$_L$ | 0.7782   | 0.5332    | 0.3317   |
| B$_M$ | −0.9681  | 0.1107    | 0.2249   |
| H$_L$ | 0.04522  | −0.9672   | −0.2498  |
| H$_M$ | 0.2749   | −0.3694   | −0.8877  |

[a] These unit vectors are scaled to reproduce the P, B, and H band intensity ratios in the absorption and circular dichroism (CD).

**TABLE 2: Hamiltonian Matrix for RC *Rb. sphaeroides* at 298 K[a]**

|       | P$_M$  | P$_L$  | B$_M$  | B$_L$   | H$_L$  | H$_M$  |
|-------|--------|--------|--------|---------|--------|--------|
| P$_M$ | 11610  | 395.0  | −16.0  | −104.0  | 19.9   | −4.8   |
| P$_L$ | 395.0  | 11610  | −94.4  | 2.82    | −6.8   | 18.0   |
| B$_M$ | −16.0  | −94.4  | 12220  | 19.3    | −7.5   | 95.8   |
| B$_L$ | −104.0 | 2.82   | 19.3   | 12370   | 123.1  | −7.9   |
| H$_L$ | 19.9   | −6.8   | −7.5   | 123.1   | 13020  | 3.9    |
| H$_M$ | −4.8   | 18.0   | 95.8   | −7.90   | 3.9    | 13150  |

[a] All energies are given in cm$^{-1}$. Diagonal energies are the effective energies of the monomer pigments. The couplings, calculated from the *Rps. viridis* crystal structure using the dipole approximation, are taken from ref 27.

in our recent modeling of B800−B850 EET in the peripheral light-harvesting complex (LH2).[24]

Together with knowledge of the arrangement of the pigments, the electronic couplings between pigments, the electron−phonon coupling, the energetic disorder, the vibrational modes, the spectral overlap, and the time scales of excitation transfer, it should be possible to provide a detailed picture of the energy transfer process. Electronic structure theory has been employed to estimate the electronic couplings between pigments of the reaction center.[25−39] The electron−phonon coupling and the energetic disorder are obtained from photon echo and hole burning measurements, whereas the vibrational motions that couple to the excitation are obtained from resonance Raman experiments. In the present work, we bring all this information together with the theoretical approach described in the accompanying paper to produce a detailed model for energy transfer dynamics in the RC. We report here not only quantitative predictions of the energy transfer rates (e.g., H to B, B to P) in both *Rb. sphaeroides* and *Rps. viridis*, but also a correct prediction of the temperature dependence. Furthermore, the same approach provides an accurate description of energy transfer in two mutant reaction centers.

In the accompanying paper we developed a formulation of Förster theory that allows for a calculation of energy transfer in chromophore aggregates.[40] We showed in that paper that when the spatial distribution of donors and acceptors in an assembly is such that the donor−donor, and/or acceptor−acceptor interaction introduces some perturbation to the absorption line shape, then the energy transfer rates must be calculated using a generalization of Förster theory.[40] For example, in the reaction center, the strong interactions between the two bacteriochlorophylls of the special pair perturb the absorption spectrum. The present paper examines the role of the special pair as an energy acceptor by applying the approach of the accompanying paper to wild-type and mutant bacterial reaction centers. This paper is organized as follows: In section II the model parameters used in the calculation of EET in the photosynthetic RC from *Rb. sphaeroides* are provided. A brief description of the calculation strategy is presented in section III. Our results and discussion are presented in section IV and V, respectively. We describe possible limitations to the model in section VI and close with concluding remarks in section V.

## II. Model Parameters

**A. Hamiltonian Matrix.** *i. Electronic Couplings.* The Q$_y$ transition dipole unit vectors, given in Table 1, are determined using the vector between the N atom of ring III and the N atom of ring I of each BChl. The dipole strength for the Q$_x$ transition is an order to magnitude less than that of Q$_y$; thus the Q$_y$−Q$_y$ electronic couplings dominate. Moreover, for the energy transfer processes we examine here, only Q$_y$ transitions provide significant spectral overlaps.

The interchromophore electronic coupling factor $V_{mn}$ is an essential ingredient in any theoretical model to calculate dynamics within the RC. An extensive number of calculations have addressed the couplings between the reaction center pigments.[25−39] We have elected to use the couplings reported by Won and Friesner, who calculated the electronic couplings between effective monomer states of the RC of *Rps. viridis* using the dipole approximation, and estimated the P$_M$-P$_L$ coupling by comparing simulations with experimental data.[27−30] This set of couplings (shown in Table 2) reproduces a wide range of experimental data (e.g., hole burning,[28] absorption,[27,29,30] polarized absorption,[30] and circular dichroism (CD)[27,29,30]) and reproduces many experimental results in the present simulations as will be shown. Because of a lack of reliable couplings for *Rb. sphaeroides*, we assume that the *Rps. viridis* couplings in Table 2 also apply to *Rb. sphaeroides*.

To simulate the absorption spectra as a function of temperature, the couplings between P$_L$ and P$_M$ had to be varied. We obtained values of 400 cm$^{-1}$ at 298 K, 500 cm$^{-1}$ at 200 K, 575 cm$^{-1}$ at 77 K, and 618 cm$^{-1}$ at 15 K, which reproduce the red shift of the P band in the absorption spectrum. A likely mechanism that could give rise to such a temperature dependence of the coupling is thermal contraction of the dimer.[41] Won and Friesner, who changed both site energies of P$_L$ and P$_M$ and the electronic coupling between P$_L$ and P$_M$ as a function of temperature in order to simulate the CD and absorption spectra, suggested such a temperature dependence.[27] Similarly, Scherer and Fisher increased the coupling within the special pair by 100 cm$^{-1}$ between 300 and 100 K in order to simulate the absorption spectrum of both *Rps. viridis*[34] and *Rb. sphaeroides*.[35,36]

*ii. Site Energies.* The effective monomer energies of P, B, and H are given by the diagonal values in Table 2 and are adjustable parameters in the simulations. These energies are "effective" because they are obtained empirically by reproducing the peaks of the absorption spectra. The electronic states for the bacteriochlorophylls of P$_{L,M}$ were taken to be degenerate. The relative energies between B$_M$ and B$_L$ (and H$_L$ and H$_M$) are assigned based on the experiments described below. In contrast to the special pair, the electronic site energies of B$_M$ and B$_L$ are different. Experimentally, linear dichroism and absorption measurements in WT versus *R*-26 (carotenoidless mutant) are used to assign the red-side of the B band in the WT to B$_M$.[42] In addition, the interpretation of the absorption spectrum of modified RCs, where [3-Vinyl]-13²-OH-bacteriochlorophyll *a* replaces the BChl$_a$ in the B$_M$ and B$_L$ binding sites, assigns the energy of B$_L$ to 803 nm and of B$_M$ to 812 nm.[43] A recent study of the mutant (M)H182L by King et al. also concludes that E(B$_M$) > E(B$_L$).[20] The electronic states of the bacteriopheophytins H$_{L,M}$ are also placed at different energies as evidenced by low-temperature linear dichroism measurements that resolve

Bacterial Photosynthetic Reaction Center

*J. Phys. Chem. B, Vol. 105, No. 8, 2001* **1655**

$H_L$ and $H_M$.[44] Additional evidence of different site energies for $H_L$ and $H_M$ is provided by the (M)L214H mutant, where a BChl$_a$ replaces a BPhe$_a$ in the $H_L$ binding site;[45] this shifts the absorption of the $H_L$ band to lower energy while leaving $H_M$ unchanged.[46]

To simulate the low-temperature absorption spectrum of the RC, the site energies of $P_L$ and $P_M$ change as a function of temperature: 11606 cm$^{-1}$ at 298 K and 200K, 11493 cm$^{-1}$ at 77 K and 15K. The Hamiltonian, derived at a given temperature using Table 2, is used to determine the reduced donor, $\mathbf{H}_d$, and the acceptor, $\mathbf{H}_a$, Hamiltonians as explained in the accompanying paper,[40] thereby providing the donor and acceptor states of the molecular system.

**B. Intramolecular Vibrations.** Once the electronic Hamiltonian has been diagonalized to obtain the electronic eigenstates, the nuclear motions are included. It is important to note here that these experimental vibrational modes are of the RC spectroscopic bands and not of individual monomers. Thus, we include these nuclear modes once the exciton states are determined.

The existence of accurate resonance Raman data on the RC provides both the ground-state frequencies of the modes that couple to the optical excitation and the values of the nuclear displacements associated with the excited-state potential energy surface.[47] Table IS (see Supporting Information) lists all the vibrational modes and Huang−Rhys factors, $S$, for P, B and H used in the calculation. $S$ measures the strength of the linear electron−phonon coupling that relates to the dimensionless displacement between equilibrium positions of ground and excited states, $\Delta$ via $S = \Delta^2/2$. Due to the similarity of the frequencies obtained from stimulated emission and Raman spectroscopy of P, we assume the ground and excited states have the same frequency. According to the formalism of Lee and Heller,[48−51] the time-dependent overlap of all vibrational modes provides the Franck−Condon factors, which in turn are used to determine both absorption and fluorescence line shapes according to eqs 4 and 2, (section II.C), respectively.

The Raman-active vibrations of the special pair have been studied extensively by many researchers.[52−56] The work of Boxer and Mathies provides vibrational frequencies and displacements for B, P, and H[52−55] as shown in Tables IS and IIS (see Supporting Information). Of all the frequencies assigned to P, the 33, 96, 127, and the 204 cm$^{-1}$ modes may have considerable intradimer character owing to their absence from the Raman spectrum of the oxidized special pair.[52] Four similar low-frequency modes were also resolved in the stimulated[57,58] and spontaneous[59] emission of P*. Mathies and co-workers reported a value of 2.9 for the total dimensionless displacement, which was distributed among 15 modes at room temperature.[55] Owing to the temperature dependence of the P Raman frequencies and intensities,[54] the low-temperature parameter set (Table IIS, Supporting Information) is employed in calculations of P below 100 K.

The vibrational parameters of the accessory bacteriochlorophylls originate from a 17-mode model reproducing resonance Raman cross sections of B at 278 K.[60] Again the low-frequency modes show similarity with those resolved by stimulated emission.[58] The total dimensionless displacement of ∼0.3 implies that B undergoes modest structural rearrangement from the ground to excited state, and is quite similar to the measured $S$ for a Chl-$a$ monomer.[61] Since the Raman cross sections of H and B are similar in magnitude and display similar temperature dependencies it is likely that the electronic and nuclear dynamics of H resemble those of B.[54] Thus, we use the same displace-

**TABLE 3: The Reorganization Energy, $\lambda$, and Time Scale, $\tau$, for the Gaussian Component of $M(t)$ and the fwhm of the Inhomogeneous Distribution, $\Gamma_{Inhom}$, for P, B, and H of *Rb. sphaeroides*[a]**

| | $\lambda^b$ | $\tau^c$ | $\Gamma_{inhom}$ |
|---|---|---|---|
| special pair | 100 | 60 | 170$^d$ |
| accessory BChl$_a$ | 80 | 60 | 55$^e$ |
| pheophytins | 80 | 60 | 55$^f$ |

[a] The functional form used for the time-correlation function is $M(t) = \lambda \exp(-t^2/\tau^2)$ where $\lambda$ is given in cm$^{-1}$ and $\tau$ in femtoseconds. The fwhm of the Gaussian inhomogeneous distribution relates to the standard deviation, $\sigma$, according to $\Gamma_{inhom} = \sigma 2(2 \ln 2)^{1/2}$. [b] Obtained by fitting the absorption spectrum; see text for details. [c] The $M(t)$ time constant in photon echo measurements of the RC B band.[70] [d] From hole-burning measurements in refs 67 and 68. [e] From resonance Raman excitation profiles of ref 60. [f] Assumed to be the same as the accessory BChls.

ments for H as B, and again use the frequencies determined by Raman spectroscopy.[54] The vibrational parameter sets of both B and H (Table IS, Supporting Information) are not adjusted as a function of temperature.

**C. Electron−Phonon Coupling.** The homogeneous contribution to the donor emission and acceptor absorption line shapes, or fast fluctuations compared to the time scale of energy transfer, is the next ingredient required for the theoretical model. The time scale and amplitude of the electronic energy fluctuations of a chromophore arise from the nuclear degrees of freedom of the protein−chromophore environment, which may be intramolecular (vibrational) or intermolecular in origin.[62,63] It is important to note that the contribution to the line-width arising from protein modes is often indistinguishable from that of the intramolecular vibrational modes of the chromophore. This chromophore−protein interaction information is embedded in the homogeneous line shape, characterized by the function $g(t)$, which is derived from a cumulant expansion of the response function and is given by

$$g_i(t) = i\lambda_i \int_0^t dt_1 M_i(t_1) + \langle \Delta\omega_i^2 \rangle \int_0^t dt_1 \int_0^{t_1} dt_2 M_i(t_2) \quad (1)$$

where $\lambda_i$ is the reorganization energy, $\langle \Delta\omega_i^2 \rangle^{1/2}$ is the coupling strength, $M(t)$ is the electronic energy gap correlation function, and $i$ denotes a given mode.[64] The coupling strength has a coth-($\hbar\omega/2kT$) dependence on temperature $T$, which allows use of the line shape function $g(t)$ at low temperature.

The values of the parameters used to calculate $g(t)$ for the reaction center chromophores, B, P, and H are provided in Table 3. Photon-echo[65] and hole-burning experiments[66−69] have been employed on the RC to eliminate "inhomogeneous" broadening, thereby isolating the "homogeneous" broadening contribution to the absorption spectrum. Although the energy fluctuations of solvated proteins occur over many time scales,[63] a Gaussian $M(t)$ with a 60 fs time scale corresponds to the typical time component resolved in photon echo measurements on the RC B band[70] and light-harvesting complexes.[71,72] Hole-burning measurements have been able to provide the fwhm of the "homogeneous" contribution to P, which dominates the absorption width.[65,68,73] In this regard, an absorption spectrum was calculated solely with $g(t)$ and the fwhm was matched to the resonance Raman "homogeneous" width, $\Gamma_{hom} = 200$ cm$^{-1}$of P, thereby fixing the coupling strength of the Gaussian. The same procedure could not be carried out for B and H because to our knowledge, explicit values for $\Gamma_{hom}$ have not been reported. Thus, the electron−phonon coupling strengths for B and H are treated as variable parameters in order to reproduce the RC experimental absorption.

**1656** *J. Phys. Chem. B, Vol. 105, No. 8, 2001*

Jordanides et al.

**D. Disorder.** Last, the energetic disorder, arising from fluctuations that are slow compared to the time scale of energy transfer, is included in the model. Disorder can be either diagonal, due to slightly different molecular environments, or off-diagonal, expressing a variation in the intermolecular interactions (e.g., electronic coupling). Diagonal disorder causes a spread in the transition frequencies that are offset by $\delta_i$ from the mean electronic transition frequency of each molecule $\epsilon_0$ according to $\epsilon_i = \epsilon_0 + \delta_i$. The distribution of these offsets is assumed to be Gaussian $P(\delta_i) = \exp(-\delta_i^2/2\sigma^2)/(\sigma\sqrt{2\pi})$ where $\sigma$ represents the standard deviation of the distribution. The standard deviation of the inhomogeneous distribution of P was obtained from hole-burning data.[66−69] The distribution of H is assumed to be identical to B, which was obtained from resonance Raman excitation profiles.[60] Table 3 reports the fwhm of the inhomogeneous distribution $\Gamma_{inhom}$ for all RC pigments. In general, the angular brackets indicate an average over an ensemble of pigment complexes. We assume that the off-diagonal disorder makes a negligible contribution. In addition, the diagonal disorder is assumed to be both uncorrelated between sites and temperature independent.

**E. Integrating Model Parameters to Calculate Spectra.** By employing the various parameters specified above, the methodology for each calculation of a spectrum is as follows: solve the eigenvalue equation for the molecular eigenstates, include electron−phonon coupling using the line shape function, $g(t)$, and the time-dependent overlap for each vibrational mode, which are both included in the basis of electronic stationary states. Once this has been completed for a set of six pigments, a Monte Carlo procedure, analogous to that of Fidder et al.,[74] was performed over 1000 to 2000 RC pigment complexes to obtain the ensemble averaged observable of interest for the entire molecular aggregate. Hence, time independent observables such as the absorption, emission, and CD spectra can be calculated as described below.

The fluorescence line shape for the donor D is defined by

$$f_{\mathrm{D}}(\epsilon) = \left\langle \sum_{\delta} |\mu_\delta|^2 f_\delta^{\mathrm{hom}}(\epsilon) \right\rangle \epsilon^3 \qquad (2)$$

where $\mu_\alpha$ is the transition moment of state $\alpha$ and the angular brackets denote an ensemble average over the static disorder in the site energies. The emission density of states (DOS) is given by

$$f_\delta^{\mathrm{hom}}(\epsilon) = \sum_k P(k)\mathrm{Re} \int_0^\infty \mathrm{d}t \langle k|k(t)\rangle \exp[i(\epsilon - \bar{\epsilon}_\delta^k +$$
$$2\lambda)t/\hbar] \exp[-g^*(t)] \qquad (3)$$

Here it is assumed that vibrational relaxation and thermalization have occurred prior to emission (and therefore prior to energy transfer). Again, $\lambda$ is the reorganization energy associated with the Stokes shift. The superscript "hom" specifies the line shape in the absence of disorder (i.e., homogeneous line broadening only). $k$ labels the vibrational modes, and $\langle k|k(t)\rangle$ represents the time-dependent overlap of the initial vibration $k$ with its evolution in the excited electronic state, which is a time-domain representation of the Franck−Condon factors. $\bar{\epsilon}_\delta^k$ is the electronic energy gap of the state $\delta$, adjusted for thermal population of mode $k$ in the excited electronic state. It contributes with Boltzmann weighting $P(k)$.

The absorption line shape for the acceptor A is defined by

$$a_{\mathrm{A}}(\epsilon) = \left\langle \sum_{\alpha} |\mu_\alpha|^2 a_\alpha^{\mathrm{hom}}(\epsilon) \right\rangle \epsilon \qquad (4)$$

where the absorption DOS is given by

$$a_\alpha^{\mathrm{hom}}(\epsilon) = \sum_l P(l)\mathrm{Re} \int_0^\infty \mathrm{d}t \langle l|l(t)\rangle \exp[i(\epsilon -$$
$$\epsilon_\alpha^l)t/\hbar] \exp[-g(t)] \qquad (5)$$

In eq 5, $l$ denotes the vibrational modes of the ground state.

Circular dichroism spectra were calculated using an analogous equation to 4, but replacing the transition dipole strength (i.e., $|\mu_\alpha|^2$) with the rotational strength for each exciton level $\alpha$ with excitation energy $\epsilon_\alpha$ and corresponding wavelength $\lambda_\alpha$

$$R(\epsilon_\alpha) = \frac{\pi}{2\lambda_\alpha} \sum_{i,j} \boldsymbol{R}_{ij} \cdot \langle \alpha|\vec{\mu}_i \times \vec{\mu}_j|0\rangle \qquad (6)$$

where $\boldsymbol{R}_{ij}$ is the center-to-center separation vector of molecules $i$ and $j$, which have transition moment vectors $\vec{\mu}_i$ and $\vec{\mu}_j$. These molecular orientations in the RC were determined using X-ray crystallographic structures of *Rps. viridis*[5] and *Rb. sphaeroides*.[6] We note that the accessory bacteriochlorophylls contribute a negative Cotton effect owing to their mutual orientation.

### III. EET Calculation Strategy

Although construction of a complete model for EET in the reaction center poses a great theoretical challenge, we believe our treatment, with the computational procedure diagrammed in Figure 5 of the previous paper, incorporates all the essential details for calculating energy transfer rates between the RC pigments.[40] In section III of the accompanying paper we described how to obtain the effective donor and acceptor states, $\{\delta\}$ and $\{\alpha\}$, as well as the couplings between them, $V_{\delta\alpha}$. Associated with each $\delta$-$\alpha$ pair is also a spectral overlap $J_{\delta\alpha}(\epsilon)$. By summing over all $\delta$ and $\alpha$ we collect each $V_{\delta\alpha}$ and associated $J_{\delta\alpha}(\epsilon)$, and thus their corresponding fragment of the EET rate via eq 15 of the accompanying paper.[40] We give a brief summary of the calculation strategy here; for details on how the theory is implemented to calculate EET dynamics in the RC, please see section III of the accompanying paper.[40]

Our calculation of $J_{\delta\alpha}(\epsilon)$ involves the following steps. (i) The set of multiple donors and acceptors {d} and {a} are interacted to give the sets of multiple donor and acceptor states {$\delta$} and {$\alpha$}. In this way, the theory gives the position and electronic composition of the states, which in turn affect the effective electronic couplings. (ii) Experimental data concerning the homogeneous line shapes and vibronic structure are now incorporated into the model. (iii) The $J_{\delta\alpha}(\epsilon)$ between each $\delta$ and $\alpha$ is calculated. Since the $V_{\delta\alpha}$ are small, we can use the full Hamiltonian to calculate effective donor emission line shapes and effective acceptor absorption line shapes. The advantages of this approach are that simultaneous calculation of the absorption and CD spectra can provide checks on the model Hamiltonian, and level shifts (small perturbations of the absorption band position) that arise through accumulated $\delta$−$\alpha$ interactions are properly incorporated into the $\delta$ and $\alpha$ line shapes.

For energy transfer from $B_L$ and $B_M$ to the special pair dimer of bacteriochlorophylls, there are two possible donor states that we label $B_+$ and $B_-$ and two possible acceptor states, $P_+$ and $P_-$. At 298 K the effective donors for *Rb. sphaeroides* are calculated to be $|B_-\rangle = -0.1419|B_L\rangle + 0.9842|B_M\rangle - 0.1015|H_M\rangle$ and $|B_+\rangle = 0.9721|B_L\rangle + 0.1452|B_M\rangle - 0.1785|H_L\rangle$, whereas the effective acceptors are $|P_-\rangle = -0.7071|P_M\rangle + 0.7070|P_L\rangle$ and $|P_+\rangle = -0.7070|P_M\rangle - 0.7071|P_L\rangle$. These effective states are not always physically meaningful, but form a convenient basis set for our calculations. $B_+$ and $B_-$ are a

Bacterial Photosynthetic Reaction Center

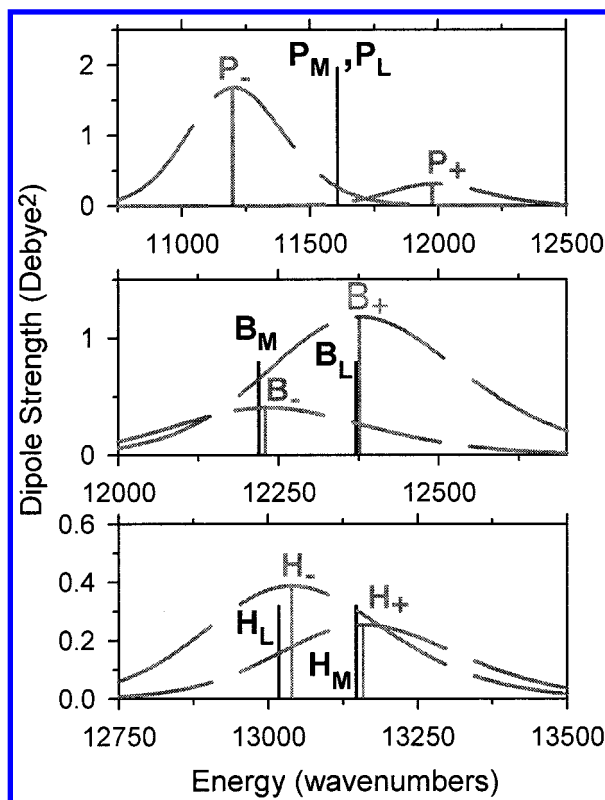*J. Phys. Chem. B, Vol. 105, No. 8, 2001* **1657**



**Figure 2.** Site energies (heavy bars), eigenstate energies (gray bars) and bandwidth of the hypothetical absorption spectrum (dashed lines) of the six pigments. The delocalized (exciton) representation is a suitable representation for the special pair (upper panel), whereas the localized (monomer) representation is appropriate and employed to represent the accessory bacteriochlorophylls (middle panel) and bacteriopheophytins (lower panel).
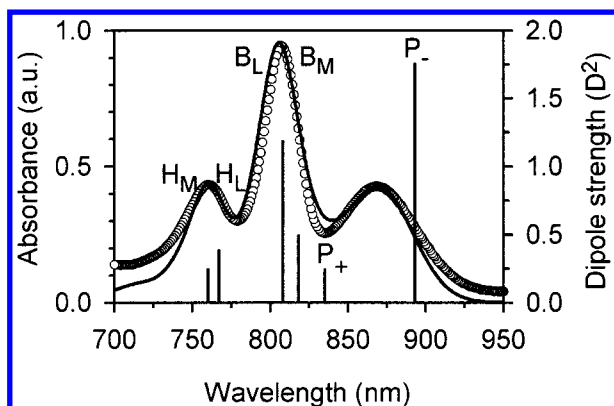


**Figure 3.** Comparison of the calculated (solid line) and experimental[75] absorption (circles) spectra for *Rb. sphaeroides* RC at 298 K. The bars indicate the relative intensities and positions of the calculated eigenstates.

case in point. We recognize that $B_+$ and $B_-$ are not the usual representations of the donor states, which are thought to be mostly localized on either $B_L$ or $B_M$, respectively. Our labeling $B_+$ and $B_-$ refers only to a basis set of electronic eigenstates. Using our basis set we need to consider four possible energy transfer pathways: $B_+$ to $P_+$, $B_+$ to $P_-$, $B_-$ to $P_+$, and $B_-$ to $P_-$. For each of these pathways, spectral overlaps $J_{\delta\alpha}(\epsilon)$ and electronic couplings $V_{\delta\alpha}$ are calculated in order to obtain the coupling weighted spectral overlap $|V_{\delta\alpha}|^2 J_{\delta\alpha}(\epsilon)$. The integrated area of this dimensionless quantity is directly proportional to the energy transfer rate. Thus, the overall rate corresponds to the sum of all four pathways $\sum_{\delta,\alpha} |V_{\delta\alpha}|^2 J_{\delta\alpha}(\epsilon)$ where donor states $\delta = B_+$ and $B_-$ and acceptor states $\alpha = P_+$ and $P_-$ weighted
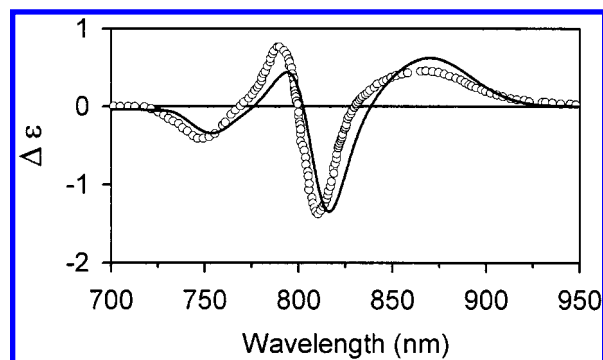


**Figure 4.** Comparison of the calculated (solid line) and experimental[90] (circles) circular dichroism spectra for *Rb. sphaeroides* RC at 298 K.
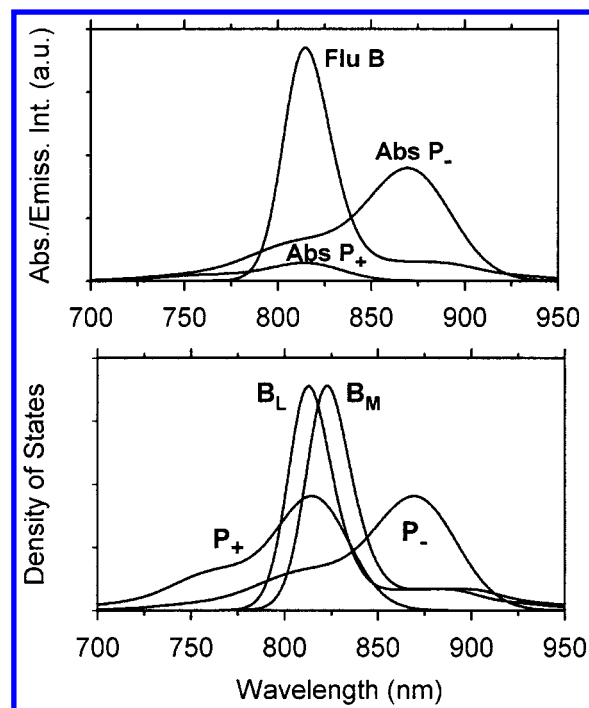


**Figure 5.** Calculated spectra and densities of states for *Rb. sphaeroides* RC at 298 K. The upper panel shows the fluorescence spectrum of the donor (Flu B) and absorption spectrum of the possible acceptors (Abs $P_+$ and/or Abs $P_-$). The lower panel shows the density of states of the donor $B_L/B_M$ and acceptor $P_+/P_-$ transitions.

by $P_\delta$, the probability of excitation being localized on either of the two possible donors, $B_L$ or $B_M$.

When discussing energy transfer for the remainder of the paper, however, we employ a physically meaningful representation that is revealed by simply looking at the absorption spectrum of the RC complex. Because of large coupling within the dimer of BChl$_a$ molecules of the special pair P, the excited state is split into upper and lower exciton states that are energetically separated by approximately twice the electronic coupling. On the basis of experimental evidence for *Rb. sphaeroides* at 10 K, the lower energy component of the pair of excitonic levels is $P_-$, whose absorption band is peaked at $\approx 890$ nm, and the higher energy component is $P_+$, with an absorption band peaked at $\approx 815$ nm.[42] Thus, we use a delocalized representation for the $P_{M,L}$ (shown in the upper panel of Figure 2) as a result of the strong electronic coupling. On the other hand, the $B_L$ contribution to the B spectroscopic band of the RC absorption spectrum has been shown experimentally to lie at higher energy than $B_M$[17,20,42,43] presumably as a consequence of different local environments.[42] Our strategy for

**TABLE 4: The Energies (in nm), Dipole Strengths (in D²), and Composition of the Exciton Eigenstates (in % of monomer contributions) at 298 K for *Rb. sphaeroides* (no disorder)**

| exciton state | energy eigenvalue | dipole strength | $P_M$ | $P_L$ | $B_L$ | $B_M$ | $H_L$ | $H_M$ |
|---|---|---|---|---|---|---|---|---|
| $P_-$ | 893 | 1.76 | 50 | 50 | 0 | 0 | 0 | 0 |
| $P_+$ | 835 | 0.25 | 45 | 44 | 3 | 8 | 0 | 0 |
| $B_-$ | 818 | 0.42 | 2 | 5 | 7 | 86 | 0 | 0 |
| $B_+$ | 808 | 1.19 | 4 | 2 | 87 | 4 | 3 | 0 |
| $H_-$ | 767 | 0.39 | 0 | 0 | 4 | 0 | 96 | 0 |
| $H_+$ | 760 | 0.24 | 0 | 0 | 0 | 1 | 0 | 99 |

the accessory bacteriochlorophylls, as shown in the middle panel of Figure 2, is to set $B_M$ and $B_L$ at different site energies. Thus, a localized representation is appropriate for $B_M$ and $B_L$ in the RC, since the electronic coupling between them is small compared to the site energy difference between them. Hence, it is important to emphasize that in the RC, energy transfer from B to P occurs from a localized donor (either $B_M$, $B_L$) to a delocalized acceptor (either $P_+$ or $P_-$). Similar to the situation with $B_M$ and $B_L$, $H_L$ and $H_M$ are localized due to the large monomer energy difference compared to their mutual electronic coupling. This situation is shown in the bottom panel of Figure 2.

The calculation of donor and acceptor states is based on the + and − (i.e., delocalized) representation, as shown by the exciton states in Table 4. By investigating the composition of these exciton states, one finds that $P_-$ and $P_+$ are delocalized over $P_M$ and $P_L$, whereas $B_-$ is 86% $B_M$, $B_+$ is 87% $B_L$, $H_+$ is 99% $H_M$, and $H_-$ is 99% $H_L$. Instead of referring to the exciton states of B and H when discussing energy transfer, we use the physically meaningful representations discussed above. For clarity, we refer to the monomer constituent that composes over 80% of each exciton state; e.g. $B_-$ will be referred to as $B_M$.

## IV. Results

**A. Steady-State Spectra.** To ensure the consistency of all parameters in the exciton model (Tables 1−4 and Tables IS and IIS, Supporting Information), we model the absorption and circular dichroism spectra. For example, the calculated room-temperature absorption spectrum is compared to the experimental data of *Rb. sphaeroides* obtained from Boxer and co-workers[75] in Figure 3. The calculated absorption spectrum reproduces all the features of the experimental spectrum. The bars or exciton sticks represent the energies and relative dipole strengths of the electronic exciton states. These energies and dipole strengths, together with the composition of the exciton states, are given in Table 4. It is important to recall that these eigenstate energies do not include the effects of homogeneous (electron−phonon and/or intramolecular vibrational) line broadening since the Hamiltonian is diagonalized with purely electronic states. As a result of phonon and vibrational modes, the maxima of the calculated spectroscopic bands are always blue-shifted with respect to the undressed eigenstates. The same model parameters give a room-temperature CD spectrum for *Rps. sphaeroides* in reasonable accord with the experimental result as shown in Figure 4.

**B. B to P EET, 298 K.** The calculated fluorescence spectrum of the donor and the absorption spectra of the potential acceptors $P_+$ and/or $P_-$ are shown in the upper panel of Figure 5. The density of states calculated for the donors $B_L$ and $B_M$ and acceptors $P_+$ and $P_-$ involved in B to P energy transfer are shown in the lower panel of Figure 5. The DOS are not weighted
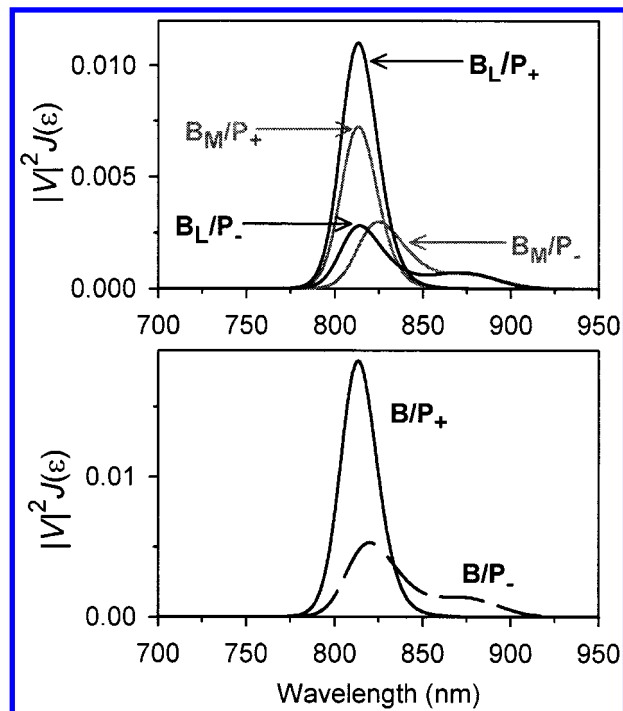


**Figure 6.** The electronic coupling weighted spectral overlaps $|V_{\delta\alpha}|^2 J_{\delta\alpha}(\epsilon)$ corresponding to the lower panel of Figure 5 and used to determine the energy transfer pathway from B to P. The upper panel shows $|V_{\delta\alpha}|^2 J_{\delta\alpha}(\epsilon)$ for each of the four possible pathways. The lower panel sums over the two possible $\delta$ = B pathways revealing that the acceptor is predominately the upper exciton state of the special pair dimer.

by the dipole strength of the transitions, thus permitting weakly allowed transitions to contribute to the available manifold of donor and acceptor states. The overlap of each B density of states with each P density of states (e.g., $B_L$ with $P_+$) provides a total of four spectral overlap functions $J_{\delta\alpha}(\epsilon)$. The corresponding overlap integrals $J_{\delta\alpha} = \int_0^\infty J_{\delta\alpha}(\epsilon)\mathrm{d}\epsilon$ are calculated to be $J_{B_L P_+} = 6.51 \times 10^{-4}$ cm, $J_{B_M P_+} = 5.82 \times 10^{-4}$ cm, $J_{B_M P_-} = 4.17 \times 10^{-4}$ cm, and $J_{B_L P_-} = 3.82 \times 10^{-4}$ cm (Recall that "$B_L$" here refers to "$B_-$," etc. as explained in section III.). Hence, the spectral overlap between B and $P_+$ is 55% larger than between B and $P_-$.

The electronic couplings $V_{\delta\alpha}$ between the donor, $\delta$ and acceptor, $\alpha$ states calculated using eq 11 of the accompanying paper[40] are given by $V_{B_L P_+} = 82.7$ cm$^{-1}$, $V_{B_M P_+} = 67.1$ cm$^{-1}$, $V_{B_M P_-} = -67.4$ cm$^{-1}$, and $V_{B_L P_-} = 68.8$ cm$^{-1}$. Clearly, the electronic coupling is quite equally distributed. Couplings to $P_-$ do not dominate over those to $P_+$ as is suggested by the dipole approximation, which relates the dipole strengths seen in the optical absorption spectrum to the couplings.[76]

To determine the energy transfer rate, each $J_{\delta\alpha}$ is weighted by the square of the electronic coupling $|V_{\delta\alpha}|^2$ to give the corresponding coupling-weighted spectral overlap $|V_{\delta\alpha}|^2 J_{\delta\alpha}(\epsilon)$ for each pathway.[24] Since $|V_{\delta\alpha}|^2 J_{\delta\alpha}(\epsilon)$ is the quantity that governs EET we can ascertain the most significant electronic states by comparing values of $\int d\epsilon |V_{\delta\alpha}|^2 J_{\delta\alpha}(\epsilon)$, which are directly proportional to the rate for each pathway as pictured for B to P energy transfer in the upper panel of Figure 6. When a sum over the two donor B states is taken so as to obtain the average B to P EET times, the $\sum_\delta P_\delta |V_{\delta\alpha}|^2 J_{\delta\alpha}(\epsilon)$ are given by the lower panel of Figure 6. The B/$P_+$ contribution to $|V_{\delta\alpha}|^2 J_{\delta\alpha}(\epsilon)$ is significantly larger in area than the B/$P_-$ contribution, which clearly shows that energy transfer from B to P occurs primarily from B ($B_M$ or $B_L$) to $P_+$. The calculated EET times at 298 K

Bacterial Photosynthetic Reaction Center

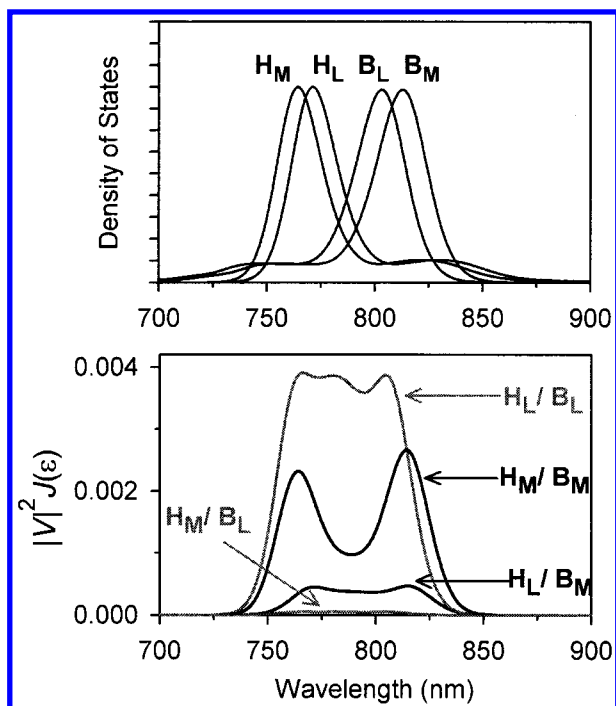*J. Phys. Chem. B, Vol. 105, No. 8, 2001* **1659**



**Figure 7.** Calculation results for energy transfer from H to B *Rb. sphaeroides* RC at 298 K. The density of states (upper panel) and the corresponding electronic coupling weighted spectral overlaps $|V_{\delta\alpha}|^2 J_{\delta\alpha}(\epsilon)$ for the donor $H_L/H_M$ and acceptor $B_L/B_M$ eigenstates (lower panel) are shown.

for *Rb. sphaeroides* are 190 fs from $B_L$ to $P_+$, 322 fs from $B_M$ to $P_+$, 445 fs from $B_M$ to $P_-$, 467 fs from $B_L$ to $P_-$. These calculations provide quantitative support that the $P_+$ pathway is the dominant, but not exclusive pathway. Experimentally, exclusive preparation of the electronic states $B_L$ and $B_M$ is not generally possible; thus, in the Discussion section we devise a kinetic model to compare our calculated rates with the experimental observables.

**C. H to P EET, 298 K.** There are two possible pathways by which energy can be transferred from H to P: (1) sequentially, i.e., H to B followed by B to P, and (2) H to P direct transfer, where B is not directly populated. The electronic couplings and spectral overlaps for H to P direct transfer are both small. Hence, our calculations show that EET occurs by a sequential pathway as will be discussed below.

Calculation of the H to B electronic couplings $V_{\delta\alpha}$ yields the following: $V_{H_LB_L} = -113.2$ cm$^{-1}$, $V_{H_MB_M} = -87.5$ cm$^{-1}$, $V_{H_LB_M} = -38.7$ cm$^{-1}$, and $V_{H_MB_L} = 13.0$ cm$^{-1}$ (Recall again that "$B_L$" here refers to "$B_-$," etc. as explained in section III.). The active branch bacteriopheophytin and bacteriochlorophyll pigments have the largest electronic coupling of the four. The density of states of the B acceptor states and the H donor states are shown in Figure 7 (upper panel) and the associated spectral overlaps $J_{\delta\alpha}$ between H and B are calculated to be the following: $J_{H_LB_L} = 3.90 \times 10^{-4}$ cm, $J_{H_MB_M} = 2.97 \times 10^{-4}$, $J_{H_LB_M} = 3.13 \times 10^{-4}$ cm, and $J_{H_MB_L} = 3.22 \times 10^{-4}$ cm. Obviously the two states with the smallest energy difference, $B_L$ and $H_L$, have the greatest spectral overlap. In addition, the importance of the vibrational contribution to the spectral overlaps can be seen in upper panel of Figure 7 where the DOS maximum of the electronic transition of the donor (acceptor) overlaps with the vibronic shoulder of the acceptor (donor) DOS. As a result, the calculated $J_{\delta\alpha}(\epsilon)$ and similarly $|V_{\delta\alpha}|^2 J_{\delta\alpha}(\epsilon)$ of Figure 7, are comprised of not merely one peak at $\approx 800$ nm, but rather a broad band from $\approx 750$ nm to $\approx 840$ nm.
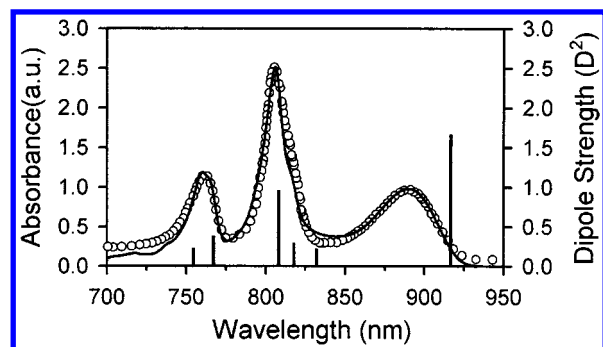


**Figure 8.** Comparison of the calculated (solid line) and experimental (circles)[75] absorption spectra for *Rb. sphaeroides* RC at 77 K. The bars indicate the intensities and positions of the calculated eigenstates.

Examination of the $|V_{\delta\alpha}|^2 J_{\delta\alpha}(\epsilon)$ for the H to B active branch EET pathway, shown in the bottom panel of Figure 7, suggests that the active branch pigments provide the dominant route for energy transfer from H to B. In fact, if $H_M$ is excited the energy transfer time to $B_M$ is 371 fs, whereas if $H_L$ is excited, energy transfer to $B_L$ occurs in 165 fs. The EET times calculated for the other two pathways are 1.80 ps from $H_L$ to $B_M$ and 15.4 ps from $H_M$ to $B_L$. With these four H to B EET times and the B to P EET times from the previous section, we can solve the kinetic scheme to calculate the population kinetics from H to P. This is described in section V.C and allows a comparison between our calculations and experiments.

**D. Temperature Dependence of B to P EET.** As discussed earlier, to simulate the low-temperature absorption spectrum, (i) the site energies of $P_L$ and $P_M$ were adjusted, (ii) the electronic coupling within the special pair was increased, (iii) the vibrational frequencies of P were altered (see Table IIS, Supporting Information), and (iv) the coupling strength, or thermal component of the electron–phonon coupling contributing to the line broadening, was recalculated (see eq 1).

With the above considerations, the B to P energy transfer dynamics can be calculated at any temperature. The 77 K experimental absorption spectrum[75] is compared to the calculated spectrum in Figure 8. The electronic exciton states are also shown. Increased electronic mixing occurs between the pigments at lower temperature compared to room temperature. For example, at 15 K the upper exciton state has 21% B character, while at 298 K the upper exciton state has 8% B character. Our calculations give the location of $P_+$ as a function of temperature to be: 814 nm at 298 K, 810 nm at 77 K, and 807 nm at 15 K. As will be discussed in section V.A, these values agree with most experimental results.[42,43,65,66]

As a function of temperature the EET times for the fastest of the four pathways from B to P, i.e., $B_L$ to $P_+$ are 189 fs (298 K), 174 fs (200 K), 167 fs (77 K), and 159 fs (15 K). The rest are provided in Table IIIS, Supporting Information. The increase in the EET rate for the $B_L$ to $P_+$ pathway as the temperature is lowered originates from an increase in the largest spectral overlap $J_{B_LP_+}$. Even though $J_{B_LP_-}$, $J_{B_MP_-}$, and $J_{B_MP_+}$ decrease as a function of decreasing temperature, $J_{B_LP_+}$ increases from 6.51 $\times 10^{-4}$ cm at 298 K to 7.77 $\times 10^{-4}$ cm at 15 K. Because of the larger energy gap between $P_+$ and $P_-$ at lower temperatures, calculated here to be 800 cm$^{-1}$ at 298 K and 1200 cm$^{-1}$ at 15 K, at 15 K the maximum of the $P_+$ DOS blue-shifts to overlap with the maximum of the $B_L$ DOS, thereby increasing the term $J_{B_LP_+}$ (see bottom panel of Figure 5). On the other hand, the maximum of the $P_-$ DOS red-shifts as the temperature is lowered; this decreases the spectral overlap between the $P_-$ DOS and either the $B_M$ DOS or the $B_L$ DOS as the temperature is
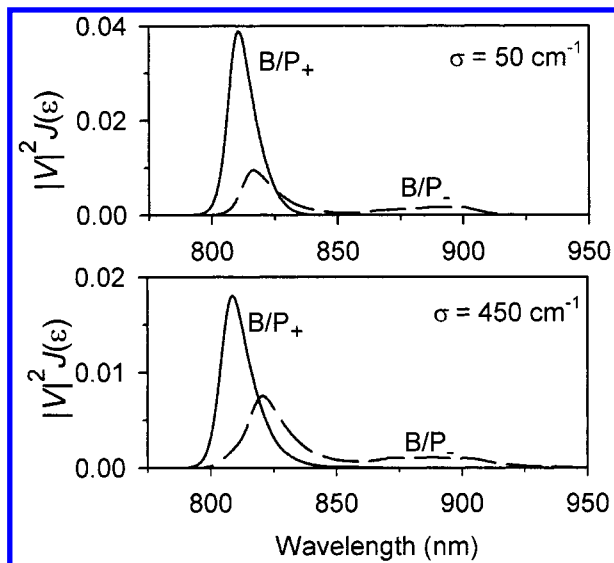
**Figure 9.** Plots of $|V|^2J(\epsilon)$ for the overall coupling pathway mediating B → P EET in the *Rb. sphaeroides* RC at 77 K. The solid line represents a calculation for B → P$_+$ EET and the dot−dash line represents B → P$_-$ EET. Disorder for the P pigments is a Gaussian distribution with (upper panel) $\sigma = 50$ cm$^{-1}$ and (lower panel) $\sigma = 450$ cm$^{-1}$. The electronic coupling within the special pair is 575 cm$^{-1}$.

lowered, but this is not enough to alter the overall EET rate since it is dominated by the B$_{M,L}$ to P$_+$ pathways.

**E. Role of Disorder.** The calculated B to P and H to B energy transfer times in the RC at room temperature only changes by 1 fs when energetic disorder is included in the calculation. A minor exception to this is for direct H to P energy transfer where ensemble averaging over 2000 molecules increases the energy transfer rate by 7% with disorder relative to that without. This is a result of the much smaller spectral overlap between H and P than between the other RC pigments. At low temperatures, where the spectroscopic bands narrow and P band red-shifts, disorder can potentially have a more significant role in the energy transfer within the RC. However, even at 15 K the effect is small, e.g., the calculated EET times from B to P and H to B are altered by 2%, while direct H to P changes by 8% when an inhomogeneous distribution of site energies is incorporated for all pigments. Therefore, disorder can be neglected in the description of energy transfer from B to P or H to B, and cannot be used to rationalize the temperature independence of the EET rates. This observation is in marked contrast to our studies of the peripheral light-harvesting antenna (LH2), where the calculated B800 to B850 energy transfer time at 50 K increased by a factor of 3 when disorder is included.[24]

In Figure 9 we show the $|V_{\delta\alpha}|^2J_{\delta\alpha}(\epsilon)$ for two of the coupling pathways for B → P EET at 77 K in the RC. We compare here calculations where disorder is represented by a Gaussian distribution with $\sigma = 50$ cm$^{-1}$ (upper panel) to those with $\sigma = 450$ cm$^{-1}$ (lower panel). Even when the disorder in the calculation is on the order of the coupling within the special pair bacteriochlorophylls (575 cm$^{-1}$), i.e., $\sigma = 450$ cm$^{-1}$, pairwise rates are not recovered, i.e., the EET still does not look like B$_M$ to P$_M$, etc. Instead, the special pair dimer must still be considered the energy acceptor. In the calculation with the larger disorder, it can be seen that the two $|V_{\delta\alpha}|^2J_{\delta\alpha}(\epsilon)$ profiles for B to P$_+$ and B to P$_-$ are more similar than with the smaller disorder, but B to P$_+$ still has a larger integrated area.

**F. *Rps. viridis*.** We calculate the EET dynamics in the *Rps. viridis* RC by altering the following with respect to the *Rb. sphaeroides* calculation: site energies of the pigments, the
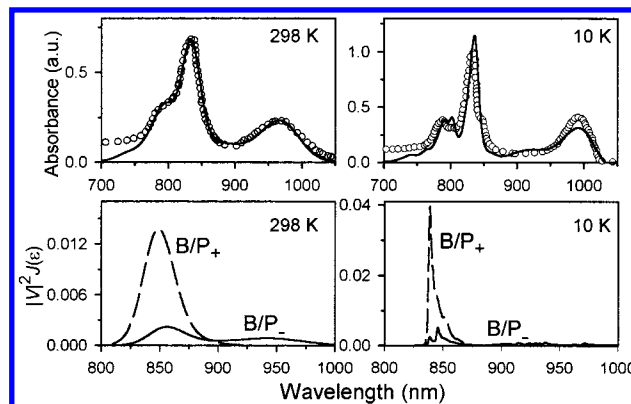


**Figure 10.** Comparison of the calculated (solid line) and experimental[3] absorption (circles) spectra for *Rps. viridis* RC at 298 K (upper left) and at 10 K (upper right). The electronic coupling weighted spectral overlaps $|V_{\delta\alpha}|^2J_{\delta\alpha}(\epsilon)$, after summing of the two donor B states, are also shown at 298 K (lower left panel) and 10 K (lower right panel).

electronic coupling within the special pair dimer, the energetic disorder, and one of the low-frequency modes of the special pair. The Hamiltonian matrix for the reaction center of *Rps. viridis* at 298 K is similar to Table 2 with these modifications: $E(P_{L,M}) = 10670$ cm$^{-1}$, $E(B_L) = 11940$ cm$^{-1}$, $E(B_M) = 11840$ cm$^{-1}$, $E(H_L) = 12390$ cm$^{-1}$, $E(H_M) = 12620$ cm$^{-1}$, and $V(P_L - P_M) = 645.0$ cm$^{-1}$. In *Rps. viridis*, the monomer site energies for P$_L$ and P$_M$ and the electronic coupling between them as a function of temperature are as follows: $V = 700$ cm$^{-1}$ ($E = 10\,650$ cm$^{-1}$) at 200 K, $V = 750$ cm$^{-1}$ ($E = 10\,640$ cm$^{-1}$) at 100 K, and $V = 850$ cm$^{-1}$ ($E = 10\,600$ cm$^{-1}$) at 10 K. The larger intradimer coupling in *Rps. viridis* compared to *Rb. sphaeroides* correlates with the estimated smaller separation between dimer macrocycles in *Rps. viridis*.[6] The coupling we employ within the special pair is quite similar to the 677 cm$^{-1}$ at 297 K reported by Won and Friesner,[27] and to the 650 cm$^{-1}$ at 77 K reported by Schulten and co-workers.[77] The energetic disorder, using hole-burning, was determined to be 120 cm$^{-1}$.[68,69] Because this value is 50 cm$^{-1}$ smaller than that of *Rb. sphaeroides*, the disorder can be neglected in the calculations of EET in the *Rps. viridis* RC. The last model parameter that is adjusted is the so-called special pair marker mode, which has an energy of 135 cm$^{-1}$ in *Rps. viridis*.[69]

The calculated 298 K absorption spectrum for *Rps. viridis* is compared to the experimental spectrum in Figure 10 and shows excellent agreement. A comparison between the calculated and experimental 10 K spectra, however, only reveals modest agreement, which seems to result from the inability of our line shape function, $g(t)$, to predict the correct low temperature homogeneous line shape. We can explain this only if the spectral density, $\rho(\omega)$, used to construct $g(t)$ is temperature dependent.

The calculated energy transfer times for *Rps. viridis* at room temperature are 177 fs from B$_L$ to P$_+$, 406 fs from B$_M$ to P$_+$, 682 fs from B$_M$ to P$_-$, and 1.15 ps from B$_L$ to P$_-$. The calculated H to B EET times are 92 fs from H$_L$ to B$_L$, 263 fs from H$_M$ to B$_M$, 891 from H$_L$ to B$_M$, and 6.03 ps from H$_M$ to B$_L$. As in *Rb. sphaeroides*, the dominant EET pathway from B to P is from B$_L$ to P$_+$. Experiments that claim to preferentially excite H$_M$ and observe a slower bleach in the P$_-$ band when compared to H$_L$/B excitation[16] agree with the trend in EET times calculated here.

As a function of temperature, the EET times of the fastest of the four pathways from B to P in *Rps. viridis*, i.e., B$_L$ to P$_+$ are given in Table IIIS, Supporting Information, and seem to be quite insensitive to temperature. When a sum over the two donor
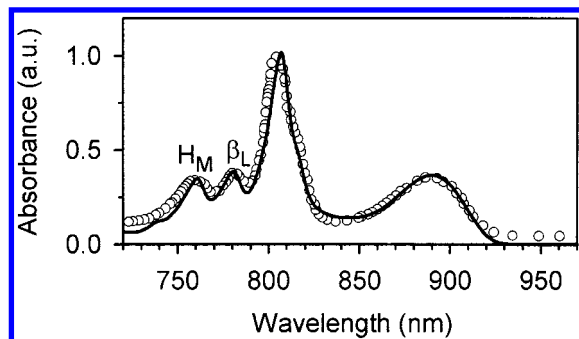
Bacterial Photosynthetic Reaction Center

*J. Phys. Chem. B, Vol. 105, No. 8, 2001* **1661**



**Figure 11.** Comparison of the calculated (solid line) and experimental[75] absorption (circles) spectra for the reaction center mutant (M)L214H (the beta mutant) at 77 K. In the beta mutant a bacteriochlorophyll *a* labeled $\beta_L$ replaces $H_L$.

B states is taken so as to obtain the average B to P EET times at 298 and 10 K, the $\sum_\delta P_\delta |V_{\delta\alpha}|^2 J_{\delta\alpha}(\epsilon)$ are given by the lower panels of Figure 10. The B/$P_+$ contribution to $|V_{\delta\alpha}|^2 J_{\delta\alpha}(\epsilon)$, at both 298 and 10 K, is significantly larger in area than the B/$P_-$ contribution, which clearly shows that $P_+$ is the primary energy acceptor in the energy transfer from B to P in *Rps. viridis*. The increase in the calculated rate of the $B_{L,M}$ to $P_+$ pathways as the temperature is lowered originates from an increase in the two largest spectral overlaps $J_{B_L P_+}$ and $J_{B_M P_+}$, whose sum increases by 31% from 298 to 10 K due to the calculated 8 nm blue-shift in the $P_+$ DOS from 298 to 10 K. On the other hand, the 27% decrease in the sum of $J_{B_L P_-}$ and $J_{B_M P_-}$ from 298 to 10 K results from the calculated 28 nm red-shift in the $P_-$ DOS from 298 to 10 K.

**G. Mutant Reaction Centers from *Rb. sphaeroides*.** *i. Beta Mutant, (M)L214H.* To test the robustness of the theory, calculations were undertaken on the mutant RC in which Leucine 214, located near the center of $H_L$, is replaced with histidine. This mutation results in the incorporation of a BChl$_a$ in place of a BPhe$_a$ in the $H_L$ binding site ($H_L$ to $\beta_L$) and this species is often referred to as the $\beta$ mutant.[45] This chromophore change is evident in the absorption spectrum at 77 K (see Figure 11) by the appearance of two bands: the $\beta_L$ band at 781 nm, and the $H_M$ at 759 nm.[13,78] The quantum yield of electron transfer from P to the primary quinone was found to be 60% less in this mutant than in the wild-type, indicating that the energetics of electron transfer are severely perturbed.[45] Energy transfer has also been studied in this mutant. EET along the active and inactive branches of the RC was compared by Boxer and co-workers, who found a somewhat slower EET time along the M side (i.e., from $H_M$ to P) than along the L side (i.e., from $\beta_L$ to P).[13]

To calculate the energy transfer rate in the $\beta$ mutant, all the model parameters are assumed to be identical to the wild-type, with the exception of the site energies, electronic couplings, and dipole strengths of the altered pigment. The former pigment $H_L$ is changed to a bacteriochlorophyll labeled $\beta_L$, which corresponds to a decrease in energy from 13020 to 12730 cm$^{-1}$ in our calculation. In addition, the increase in the oscillator strength when changing from BPhe$_a$ to BChl$_a$ is $\approx$ 20−30% as judged by comparing the spectra of the pigments in ether.[79] This change corresponds to an increase in the transition dipole moment by $\approx$10−14%; accordingly we increase the electronic couplings to the $\beta_L$ pigment by 12%.[80] In addition, the site energy of $H_M$ is decreased by 32 cm$^{-1}$. The calculated absorption spectrum at 77 K is compared to the experimental spectrum in Figure 11 and appears to be in satisfactory agreement. The calculated energy transfer time from $\beta_L$ to B is 101 fs and from $H_M$ to B is 375 fs.
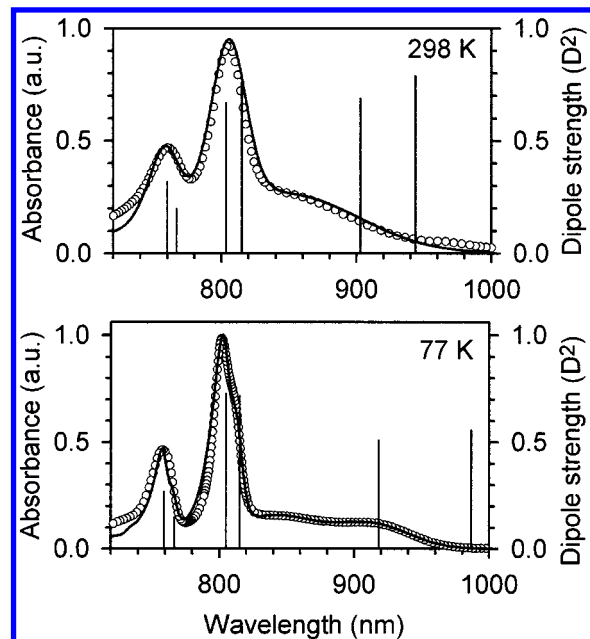


**Figure 12.** The calculated (solid line) and experimental[75] absorption spectra of the reaction center mutant (M)H202L (heterodimer) at 298 K (top panel) and 77 K (lower panel). The calculated exciton states are also depicted for the heterodimer mutant, where a bacteriopheophytin *a* replaces $P_M$ of the special pair.

*ii. Heterodimer, (M)H202L.* Of the large number of site-directed mutations in the *Rb. sphaeroides* RC, the heterodimer, where a leucine replaces the histidine that coordinates $P_M$ of the special pair, is one of the most widely studied.[17,81−86] As a result of this particular mutation, the Mg$^{2+}$ ion is lost and a bacteriopheophytin replaces $P_M$, thus creating the special pair heterodimer BPhe$_M$−BChl$_L$, commonly denoted $D_M$−$D_L$ in order to differentiate it from $P_M$−$P_L$.[83] The larger spread in energy of the heterodimer D absorption band, evident in the absorption spectrum shown in Figure 12, has been suggested to arise from a large distribution of distances between the two halves of the heterodimer,[84,85] and/or larger coupling to charge transfer states than in the wild-type as a result of electronic asymmetry.[84,87] A crystallographic analysis of the heterodimer reveals that replacement of $P_M$ with bacteriopheophytin causes no significant structural perturbations.[81] Hammes et al. used Stark spectroscopy and the low-temperature absorption spectrum of D to resolve two bands at $\approx$850 nm and $\approx$920 nm.[86] Though these bands were initially suggested to be the upper and lower excitonic states of D[86] with perpendicular transition moments, more recent fluorescence anisotropy data suggests that the two states have parallel transition moments.[17] Interpretation of resonance Raman spectrum of the (M)H202L mutant suggests that the 850 nm band is excitonic in nature.[82]

A change in the electronic couplings is perhaps the most relevant result of the mutation from BChl to BPhe in the $P_M$ binding site. From the drastic alteration of the CD spectrum of *Rb. capsulatus* heterodimer, Breton et al. inferred reduced couplings between all the chromophores.[85] Moreover, the absence of a negative LD component in the usual region of $P_+$ indicates reduced coupling between $D_L$ and $D_M$.[85] Due to the fact that the $Q_y$ dipole strength of BPhe is lower than that of BChl, one can predict reduced coupling between the BChl-BPhe dimer compared to a dimer of BChls in addition to predicting reduced coupling between the BPhe in the $D_M$ binding site and the rest of the pigments. Hammes et al. estimated that the coupling within D is reduced by at least a factor of 2 from that

within P, based on the different transition energies and oscillator strengths of B and H.[86] In addition, EET measurements on the heterodimer performed by King et al. suggest the possibility of electronic couplings that differ from the wild-type between the chromophores along the active branch.[17]

With the above experimental observations in mind, we can model the EET dynamics in the heterodimer RC using a minimum set of adjustable parameters. The site energies of the accessory BChls are shifted to the following: $E(B_M) = 12280$ $cm^{-1}$ and $E(B_L) = 12440$ $cm^{-1}$ because the absorption band of B in the heterodimer is shifted from a maximum of 805 nm in the wild-type to 802 nm. However, the energy difference between $B_M$ and $B_L$ in (M)H202L is the same as in the wild-type RC. At room temperature the site energies are $D_L$ at 10710 $cm^{-1}$, and $D_M$ at 11010 $cm^{-1}$, which have an energy difference similar to the difference in $Q_y$ transition energies of BPhe$_a$ and BChl$_a$ in solution. At 77 K, the D region has a flatter plateau and we assign the site energies of $D_L$ to be 10230 $cm^{-1}$ and of $D_M$ to be 10810 $cm^{-1}$. In accordance with the suggestion of Hammes et al.,[86] the electronic coupling between $D_L$ and $D_M$ is taken to be half the value of the wild-type, thus $V_{D_L D_M}$ at 298 K is 200 $cm^{-1}$ and at 77 K is 287 $cm^{-1}$. In addition, the couplings between $D_M$, and all the other RC pigments are halved. The line broadening functions for D are adjusted to fit the 77 and 298 K absorption spectra in the region of D. This requires a $g(t)$ with $\lambda = 800$ $cm^{-1}$ for the 850 nm feature and a $g(t)$ with $\lambda = 600$ $cm^{-1}$ for the 920 nm feature, which corresponds with the general trend of the fwhms reported by Hammes et al.[86] The large homogeneous widths, compared to $\lambda = 100$ $cm^{-1}$ of the wild-type, are essential to reproduce the broad plateau-like region in the spectrum from 820 to 980 nm.

Using these input parameters, the room-temperature absorption spectrum was calculated and is compared with the experimental results[75] in Figure 12 (upper panel). At 298 K, the lowest energy exciton state is composed of 78% $D_L$ and 22% $D_M$, while the second lowest energy exciton state is 22% $D_L$ and 78% $D_M$. Their transition moments were calculated to have an angle of 27 degrees between them. The exciton states of the heterodimer special pair are different from the wild-type because there is no longer a 50:50 excitonic mix between D states. With the inclusion of line broadening in the calculation, these absorption features peak at 832 and 866 nm. The calculated CD spectrum has only two bands − one of positive ellipticity and one of negative ellipticity − similar to the CD reported for the *Rb. capsulatus* heterodimer.[85] By summing the calculated EET rates from $B_M$ (or $B_L$) to the two acceptor D states, the EET times are calculated to be 233 fs from $B_M$ to D and 810 fs from $B_L$ to D.

In the lower panel of Figure 12, the calculated 77 K absorption spectrum and the experimental absorption spectrum[75] are shown. At this lower temperature, where the site energy difference is larger, the two lowest energy exciton states are even more localized on either D, i.e., the 987 nm state is composed of 88% $D_L$ and 12% $D_M$ character and the 918 nm state is 12% $D_L$ and 88% $D_M$. Once the homogeneous line shapes are included, the densities of states corresponding to these exciton sticks are blue-shifted to 835 and 910 nm, respectively. This is shown in the density of states plot in the upper panel of Figure 13. Because the positions of these states are not as well determined as they are in the wild-type, there is a larger uncertainty in the calculated energy transfer rate. The four possible $|V_{\delta\alpha}|^2 J_{\delta\alpha}(\epsilon)$ are shown in the lower panel of Figure 13. This figure reveals that the M side dominates the energy transfer to D.
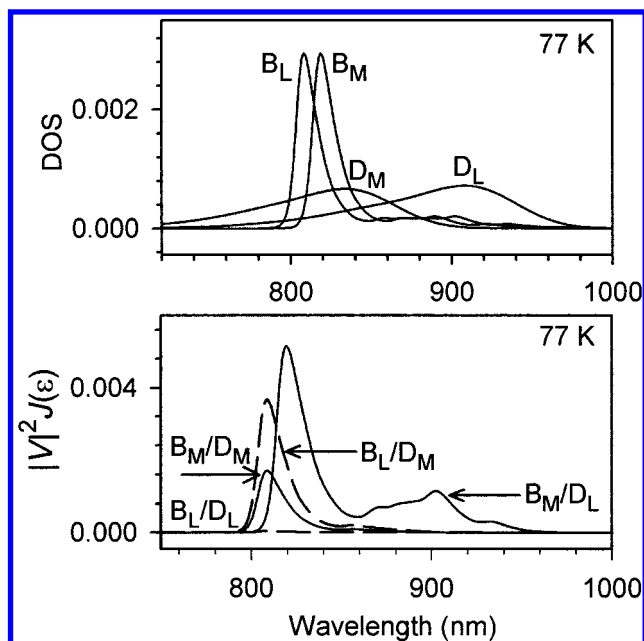


**Figure 13.** Calculation results for energy transfer from B to D for the heterodimer mutant at 77 K. The density of states (upper panel) and the corresponding electronic coupling weighted spectral overlaps $|V_{\delta\alpha}|^2 J_{\delta\alpha}(\epsilon)$ for the donor $B_L/B_M$ and acceptor $D_M/D_L$ eigenstates (lower panel) are shown.

**H. The Effects of Excess Vibrational Excitation.** The possibility that B to P or H to P EET proceeds from an unrelaxed, vibrationally hot, initial donor excited state has been previously suggested.[10,14,16] It is possible that vibrational relaxation competes with the energy transfer from either H or B to P. Recently, it has been shown for *Rb. sphaeroides* at 298 K that there is an excitation wavelength dependence of the RC spectral evolution, and that the amplitude of stimulated emission from P* is roughly 20% less when H or B are excited than when P is excited.[14] One possible origin of these experimental observations is incomplete vibrational relaxation of B and/or H on the time scale of energy transfer to P.[14]

To investigate whether incomplete thermal equilibration in the electronically excited state of the donor significantly affects the time scale of EET, we calculated energy transfer from a thermalized, vibrationally hot (1200 K) donor bacteriochlorophyll excited state to a thermalized (298 K) acceptor special pair ground state. The distribution of B vibrational populations at 1200 K corresponds to an excess vibrational energy of 834 $cm^{-1}$ compared to those equilibrated at 298 K, which corresponds to 207 $cm^{-1}$ of excess energy. Although the distribution of vibrational populations drastically changes as a function of temperature, the calculated EET time increases by only 3 fs at the higher temperature. Hence, we do not expect the B to P EET rate to be significantly affected by the dynamics of vibrational relaxation and thermal equilibration in the donor excited state.

## V. Discussion

**A. Steady-State Spectra.** It is difficult to determine precisely the $P_+$ position at room temperature because of the large electron−phonon coupling and overlap of the bands. Accordingly, the position of the upper exciton component has been the subject of extensive debate,[19,20,42−44,65,66,88] which will be summarized below for the RC from *Rb. sphaeroides*. Using linear dichroism, the studies by Breton et al. at 15 K[42] and Beekman et al. at 77 K[88] estimated $P_+$ to lie at 814 and 815

Bacterial Photosynthetic Reaction Center

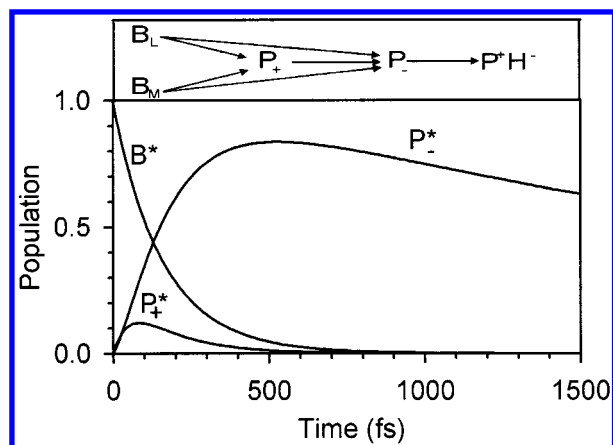*J. Phys. Chem. B, Vol. 105, No. 8, 2001* **1663**



**Figure 14.** The RC state populations (at 298 K for *Rb. sphaeroides*) calculated by employing the kinetic model shown with the calculated EET times given in the text. The B population decays with a 164 fs time constant, the $P_-$ population rises with a 193 fs time constant, and the $P_+$ population rises and decays with 48 and 158 fs time constants, respectively.

nm, respectively. A pump−probe anisotropy study at 298 K assigned it to 825 nm.[19] Photochemical hole-burning at 4.2 K assigned a feature at 811 nm to $P_+$,[66] photon echo spectra assigned it to 813 nm at 77 K,[65] and recently an 8 K absorption spectra of a modified RC, with accessory BChl$_a$ substituted by [3-vinyl]-13$^2$-OH-BChl, located $P_+$ between 805 and 810 nm at 8 K.[43] In the present study, the $P_+$ band is assigned to 814 nm at 298 K (see the maximum of the density of states of $P_+$ in bottom part of Figure 5) and blue-shifts slightly as a function of temperature (810 nm at 15 K). This assignment agrees with most of the experimental data.[42,43,65,66,88]

There are deviations between experimental and calculated CD spectra as can be seen in Figure 4. However the CD spectrum depends on RC preparation.[89] The experimental CD spectrum shown here is for *Rb. sphaeroides* R26 mutant.[90] In our calculations, the site energies of the $B_M$ and $B_L$ were optimized to agree with the experimental absorption spectra[75] that were measured for RCs from *Rb. sphaeroides* wild-type. The calculated positive ellipticity of the 790 nm band is not as large as the experimental value. If the only interactions contributing to the CD were excitonic interactions between the $Q_y$ transition dipoles of the bacteriochlorin molecules, the CD spectrum would be conservative.[91] However, the experimental CD spectrum of the RC contains more positive than negative ellipticity. Mar and Gingras discovered that the RC CD spectrum became conservative when the interactions were limited to the special pair dimer and one accessory B by trapping the rest of the pigments in doubly reduced states.[92] These workers suggested that the nonconservative CD spectrum originates from the interactions between the H and B chromophores and their local protein environments.[91] Thus, the incorrect ellipticity in the 790 nm band predicted by our calculations perhaps originates from neglect of specific protein interactions.

**B. B to P EET, 298 K.** *i. Comparison with Experiments.* Experiments do not simply measure the EET rate from B to P, but rather the decay or rise in a population. Thus, to compare the calculated electronic energy transfer rates with experimental observables, namely, the rise of the fluorescence of $P_-$ or the decay of the bleach (or emission) of B, the electronic state populations of the states in the kinetic scheme in Figure 14 are simulated and fit. The normalized populations of each state, where $[B(t)] = [B_M(t)] + [B_L(t)]$, are shown in Figure 14 for *Rb. sphaeroides* at 298 K. A monoexponential fit of the B population decay yields a time constant of 164 fs, which lies

between the ≈180 fs decay of the B bleach measured by Vos et al,[16] and the 124 fs decay at 800 nm measured by Jonas et al.[12] To calculate the kinetics of $P_-$ we assume that the rate of energy transfer rather than the rate of $P_+$ to $P_-$ internal conversion, $k_{ic}$, is rate limiting.[92] When we assume a $(k_{ic})^{-1}$ of 50 fs, the rise of the $P_-$ population is fit to a single exponential with a 193 fs time constant. For the remainder of the paper $(k_{ic})^{-1}$ will be assumed to be 50 fs. The rise of the fluorescence of $P_-$ has been measured by our group to be 120 fs at 298 K,[11] which is faster than the calculated rise times. Table 5 shows a comparison between time constants extracted from fitting the population kinetics with our calculated EET times and the experimental EET dynamics in the RC.

*ii. Electronic Couplings.* In the accompanying paper we described in detail how to calculate electronic couplings between effective donor and acceptor states in molecular aggregates.[40] The central result of that paper is that electronic couplings must account explicitly for the pairwise interactions between each molecule in the aggregate.[40] We considered the averaging over wave functions to determine the Coulombic coupling to be implemented on two levels. In the present work this reduces to two levels of implementation of the dipole approximation: (a) with respect to the coupling between sites (i.e., using the dipole approximation for pairwise couplings such as $B_M$ to $P_L$) and (b) with respect to the coupling between donor and acceptor supermolecules (e.g., $B_M$ to $P_-$). Here we have formulated the expression for the EET rate in terms of effective couplings, $V_{\delta\alpha}$, and implemented the dipole approximation only for the coupling between sites (a). As such, it is not possible to associate donor, $\delta$, or acceptor, $\alpha$, states with one molecule entirely. Using the full Hamiltonian for the RC, we obtain the effective couplings, $V_{\delta\alpha}$, listed in column 2 of Table 6. In this representation, the effective donors are mixtures of B and H, and the effective acceptors are mixtures of P and H.

To enable us to quantify the deviation of our result from that obtained from dipole−dipole couplings between monomeric $B_L$ and $B_M$ and the effective acceptor $P_+$ and $P_-$, we transform our calculated $V_{\delta\alpha}$ into a form $V_{m\alpha}$ such that the donors are truly 100% $B_M$ or $B_L$ (rather than effective donors). Given the effective donor and acceptor wave functions provided in section III, the electronic couplings between sites, $V_{mn}$, in Table 2, and the electronic couplings between effective donor and acceptor states, $V_{\delta\alpha}$, in Table 6, (column 2) a transformation from effective donors to a localized donor representation is possible. These couplings are given in column three of Table 6 and are precisely analogous to the example given in Figure 3b[40] of the accompanying paper. The effective couplings, $V_{\delta\alpha}$, differ from the pure B donor state couplings, $V_{m\alpha}$, by as much as 18%, which results from associating the donor, $\delta$, to one molecule entirely. These differences between $V_{\delta\alpha}$ and $V_{m\alpha}$ occur because the donor bacteriochlorophylls are not pure $B_L$ or $B_M$; they are slightly mixed. This mixing introduces an interference effect, which affects the net coupling between the $B_L/B_M$ and $P_+/P_-$. The interference may be constructive or destructive because individual contributions to the couplings have different signs just as in multiple pathway superexchange.[94−97] This interference is also responsible for causing the $V_{B_L P_+}$ to be the largest of the four calculated couplings, $V_{\delta\alpha}$. In the case of $V_{B_L P_+}$, there is constructive interference between the direct $B_L−P_+$ coupling and the indirect $B_L−B_M−P_+$ coupling, which results in $V_{B_L P_+}$ being larger than $V_{B_M P_+}$, where there is destructive interference between the direct and indirect pathways. For an explanation of electronic couplings that occur through multiple pathways see references[94−97] and references therein.

**TABLE 5: A Comparison between the Calculated and Experimental Electronic Energy Transfer Times Obtained from Fitting Population Dynamics in the RC[a]**

| reaction center/ *species*/temp | pathway | observable | EET times | | reference |
|---|---|---|---|---|---|
| | | | calculated[b] | experiment | |
| *Rb. sphaeroides* wild-type | | | | | |
| 298 K | B to P | [B(t)] decay | 164 | 180 | Vos et al.[16] |
| | | | | 124 | Jonas et al.[12] |
| | | [P−(t)] rise | 193 | 120 | Jonas et al.[11] |
| | H to B | [H(t)] decay | 242 | <100 | Vos et al.[16] |
| 77 K | B to P | [B(t)] decay | 173 | 160 ± 10 | King et al.[20] |
| | | [P−(t)] rise | 196 | 163 ± 54 | Stanley et al.[13,c] |
| | H to P | [P−(t)] rise | 370 | 260 ± 32 | |
| 15 K | H to B | [H(t)] decay | 266 | <100 | Vos et al.[16] |
| | B to P | [B(t)] decay | 175 | 200−300 | |
| beta mutant | | | | | |
| 77 K | $H_M$ to P | [P−(t)] rise | 480 | 300 ± 11 | Stanley et al.[13,c] |
| | $\beta_L$ to P | [P−(t)] rise | 250 | 239 ± 35 | |
| | B to P | [P−(t)] rise | 196 | 162 ± 25 | |
| heterodimer | | | | | |
| 77 K | $B_L$ to D | [D(t)] rise | 710 | 784−873 | King et al.[17,c] |
| | $B_M$ to D | [D(t)] rise | 278 | 99−139 | |
| *Rps. viridis* | | | | | |
| 298 K | B to P | [P−(t)]bleach | 215 | 90 | Vos et al.[16] |
| 10 K | B to P | [P−(t)]bleach | 192 | 80 | |

[a] All times are in femtoseconds (fs). Only the calculated EET rates, which have an experimental counterpart, are shown. [b] These numbers are obtained from a monoexponential fit of the time dependent concentrations of the kinetic scheme as explained in the text. The calculated values from H to P as a result of the quality of the fit, have a larger error, thus are reported with only two significant figures. [c] These experiments are performed at 85 K.

**TABLE 6: Calculated Electronic Couplings in the *Rb. Sphaeroides* RC at 298 K [All Couplings in Wavenumbers ($cm^{-1}$)]**

| coupled pigments | electronic couplings | | |
|---|---|---|---|
| | $V_{\delta\alpha}$[a] | $V_{m\alpha}$[b] | $V_{dd}$[c] |
| $B_M P_-$ | −67.4 | −55.4 | 198.4 |
| $B_L P_-$ | 68.8 | 75.5 | −182.1 |
| $B_M P_+$ | 67.1 | 78.0 | −6.3 |
| $B_L P_+$ | 82.7 | 71.6 | −29.0 |

[a] Effective couplings used in our calculation. [b] $B_M$ and $B_L$ are pure monomers, (see Figure 3b of the accompanying paper[40]). [c] Dipole approximation between supermolecules, e.g., between $P_+$ and $B_M$ (see Figure 3c of the accompanying paper[40]).

The dipole approximation, as used in the usual application of Förster theory ($V_{dd} \propto \kappa\mu_D\mu_A/R^3$) where the donors are monomeric $B_{L,M}$ and the acceptors are upper and lower exciton state transition dipoles of P (assumed to be a supermolecule!) produces couplings that may be directly compared with our $V_{m\alpha}$. These dipole couplings, $V_{dd}$, given in column four of Table 6, differ significantly from both the $V_{m\alpha}$ and the $V_{\delta\alpha}$ used to calculate EET in this work. Notice, for example, that at this level of description the coupling to $P_+$ is very small and the coupling to $P_-$ is large. Therefore, within the dipole approximation the electronic couplings are proportional to the transition dipole moment of the electronic transition.[98] The dipole approximation in the context of molecular aggregates, i.e., implemented at the second level above, imposes a further level of averaging such that the $P_-$ (or $P_+$) special pair state is taken to be an energy acceptor. This averaging is akin to that in optical spectroscopy. The wavelength of the probing light is large compared to the dimensions of the aggregate, so the distinction between different molecules in the aggregate and their role in the coupling between donor and acceptor is obliterated. This inability to resolve the true molecular dimensions reduces the set of two P molecules to one point in space whose coupling is determined to another point in space, a B molecule, whose coupling is given by $V_{dd}$.

So far we have focused entirely on Coulombic coupling between donors and acceptors. However, in efforts to rationalize the rapid energy transfer times observed in the reaction center, orbital overlap mediated coupling, $V_{mn}^{short}$, has been proposed by several authors.[11−13,16,21,22] The conclusion from the present work, however, is that the deficiency of the dipole−dipole coupling $V_{dd}$ is not due to discrepancies in calculating the pairwise couplings, $V_{mn}$. On the contrary, the Coulombic coupling seems quite adequate provided the donor−acceptor coupling, $V_{\delta\alpha}$, is calculated correctly. Our results suggest that $V_{mn}^{short} \ll V_{mn}^{Coul}$ for all couplings within the reaction center except $P_M−P_L$, which is reasonable considering recent calculations of the electronic couplings within the LH2 antenna complex.[99] The way that we have adapted Förster theory does not explicitly include orbital overlap effects. However, because the interactions that depend explicitly on orbital overlap are usually a nearest-neighbor interaction, we can absorb these terms into the couplings $V_{mn}$ to a good approximation. In addition our model does not explicitly include interactions with the charge transfer states; however, these are implicitly accounted for in the special pair by varying the coupling within $P_L$ and $P_M$ and their site energies. Charge transfer states between other pigments are ignored because $V_{mn}^{short}$ is expected to be very small between them[100,101]

*iii. Role of $P_+$ in the mechanism of EET from B to P.* Although not a unanimous agreement,[15] a consensus exists that the usual application of Förster theory is deficient by as much as an order of magnitude in accounting for the rate of EET between the RC cofactors.[13,14,16,21,23] This comes about from use of the $V_{dd}$ values of Table 6 which, because $P_-$ carries 88% of the dipole strength, shows strong coupling to B despite the small overlap with the B emission. On the other hand, the upper exciton state $P_+$ overlaps significantly with the B emission, but since it carries only 12% of the total dipole strength, it has small $V_{dd}$ values. Table 6 clearly implies that EET predominantly occurs from B to $P_-$ at the level of $V_{dd}$. Our adaptation of Förster theory not only gives a much-improved quantitative agreement with

Bacterial Photosynthetic Reaction Center

*J. Phys. Chem. B, Vol. 105, No. 8, 2001* **1665**

experiment, but a different physical picture than that suggested by the usual application of Förster theory emerges. Our more detailed model suggests that a weak-coupling mechanism, in which the energy transfer is dominated by the B $\rightarrow$ P$_+$($\rightarrow$P$_-$) pathway, provides an adequate description.

Some researchers have previously suggested the involvement of P$_+$ in mediating EET from B to P$_-$,[10,12,16,21] but others considered it to be less important than direct energy transfer to P$_-$.[9,15,17,18] A Förster calculation by Hochstrasser and co-workers,[15] based on the couplings of Scherer and Fischer,[35,36] suggested that there is sufficient spectral overlap between the B$_L$ emission and the P$_-$ absorption to achieve an EET time of 158 fs for the active branch.[15] However, the Scherer and Fischer Hamiltonian differs significantly from the one we have used. The theoretical analysis of the absorption and CD spectra by Scherer and Fischer for *Rb. sphaeroides* results in an eigenstate representation that heavily mixes B and P$_+$ and assigns the band with most P$_+$ character to 776 nm. In addition, the exciton states B$_-$ (at 798 nm) and B$_+$ (at 807 nm) were sandwiched between P$_+$ (776 nm) and P$_-$ (859 nm).[35,36] Using their electronic couplings (and allowing the site energies to vary in order to fit the absorption and CD spectra), we calculated a similar energy ordering of the exciton states, which is in serious disagreement with the experimentally determined location of the BChl$_a$ and the P$_+$ bands.[42,43,66,65] Therefore, we believe that the model used by Scherer and Fischer[35,36] incorrectly places P$_+$ at higher energy, 776 nm, than B$_-$ and B$_+$. Nonetheless, if we use the Scherer and Fischer Hamiltonian to calculate the EET rate, the decay of the B population is 202 fs and is dominated by electronic interaction and spectral overlap between B and P$_-$. Of course, in this model P$_-$ plays the dominant role in EET from B to P.

The faster calculated energy transfer times, compared to previous estimates, can be partially attributed to the improved spectral overlap used throughout this work. The large displacements of the special pair intramolecular vibrational modes[55] result in a vibronic manifold on the blue edge of the acceptor P (or B) density of states providing significant spectral overlap with the donor B (or H) density of states as shown in Figures 5 -7. Using the experimental line shapes, the spectral overlaps at 298 K are calculated to increase the rate of EET from B to P by a factor of 3 over that calculated with Gaussian line shapes. Another factor that could affect $J_{BP_+}$ is the Stokes shift of B. If we take the Stokes shift of B to be precisely zero on the time scale of EET, as reported by King et al.,[20] then we calculate an energy transfer time from B to P in *Rb. sphaeroides* that is 2% slower than the EET rate calculated with our original parameters. Thus, we find that our conclusions are not critically dependent upon the exact position of B or P$_+$.

The results of our EET calculations from B to P can be summarized as follows: (1) using our detailed vibrational line shapes to determine $J_{\delta\alpha}(\epsilon)$ decreases the calculated Förster EET times to $\approx 1$ ps from the $\approx 3$ ps reported previously,[21] and (2) the calculated $\approx 200$ fs rise time of the P$_-$ population, in good agreement with experiment, can only be obtained using our generalized Förster theory which incorporates a proper calculation of $V_{\delta\alpha}$.

**C. H to P EET, 77 K.** In a one-step energy transfer pathway from H to P, where B merely acts as a bridge to allow electronic mixing with both H and P, (e.g., superexchange) the calculated rate of direct H to P EET obtained from fitting the decay of H in the kinetic scheme H $\rightarrow$ P is 8.06 ps at 77 K. Hence, this calculation clearly suggests, as expected,[13,16] that *B* is a real intermediate in the energy transfer from H to P.
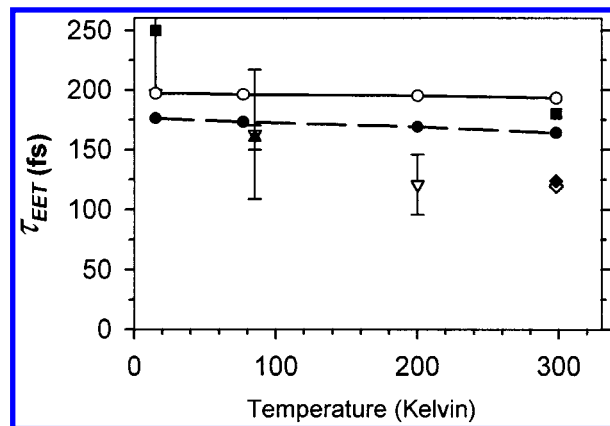


**Figure 15.** The calculated and experimental temperature dependence of the B population decay (dashed line with filled circles) and of the P$_-$ population rise (solid line with open circles), representing EET from B to P in *Rb. sphaeroides*, are shown. The experimental P$_-$ rise times (open symbols) have the following origins: the triangles at 85 and 200 K are from ref 13 and the diamond at 298 K is from refs 10 and 11. The experimental B decay times (solid symbols) have the following origins: the squares 10 and 298 K are from ref 16, the triangle at 85 K is from ref 20, and the diamond at 298 K is from ref 12.

To compare our calculations with experiments that measure the P$_-$ fluorescence, we add the two states (H$_M$, H$_L$) and four possible pathways to the kinetic scheme in Figure 14, and, with the initial condition [H($t$=0)] = 1, solve for [P$_-$($t$)]. After fitting the rise of the P$_-$ population to a monoexponential, a time constant of $\approx 370$ fs is retrieved, which is 90% longer than rise of the P population determined if [B($t$=0)] = 1. Experimentally (at 85 K) upon excitation of H the fluorescence of P$_-$ has a rise time of $\approx 260$ fs, or 50% longer than the rise of P$_-$ fluorescence after excitation of B.[13] By fitting the decay of H in the kinetic scheme H $\rightarrow$ B to a monoexponential, a decay time of 256 fs at 77 K is obtained. However, recent experiments using fluorescence upconversion at 85 K yield H to B energy transfer times of 80−160 fs.[20] Although our results are in general accord with these experimental findings, we do not predict the correct relative rates for H to B and B to P in *Rb. sphaeroides*. Our calculated H to B energy transfer times are two times longer than the experimental values, which causes the corresponding difference in the calculated and measured rise times of P$_-$. Trial calculations suggest that the source of error is in $V_{mn}$, in particular $V_{HB}$, rather than $J$, which cannot be varied much. Hence, the electronic coupling matrix may need adjustment from the values calculated in ref 27, we will not attempt to do so here.

**D. Temperature Dependence of B to P EET.** According to the method of the previous sections, the calculated EET times are used as inputs into a kinetic model for comparison with experiments. By fitting the decay of B, the extracted decay times are 164 fs at 298 K, 169 fs at 200 K, 173 fs at 77 K, and 176 fs at 15 K, and are shown in Figure 15 by the dashed line with circles. By assuming that $(k_{ic})^{-1}$ is 50 fs, we obtained rise times for P$_-$, which represent EET from B to P, of 193 fs at 298 K, 195 fs at 200 K, 196 fs at 77 K, and 197 fs at 15 K. These results are depicted in Figure 15 by the solid line and both sets of calculated times, although somewhat longer, compare well with experiments. The rise times of the P$_-$ populations are more insensitive to temperature because they are a function of $k_{ic}$, which is assumed to be temperature independent.

In our calculations, we assume that protein contraction at low-temperature reduces the separation between P$_L$ and P$_M$, which correspondingly increases $V$(P$_L$–P$_M$) as the temperature decreases. Despite this change of the electronic coupling within

the special pair as a function of temperature, the electronic coupling between effective donors and acceptors $V_{\delta\alpha}$ do not change as a function of temperature;[102] therefore, the temperature dependence of EET originates from $J_{BP}$. One would expect that the unusual behavior of the P$_-$ absorption band as a function of temperature—the peak is blue shifted from 894 nm at 15 K to 870 nm at 298 K—to have dramatic consequences on the temperature dependence of EET. This is not the case because the EET rate from B to P is dominated by the spectral overlap between the B DOS and the upper exciton state P$_+$.

**E. *Rps. viridis*.** The location of the upper exciton state of the special pair in *Rps. viridis* is also the subject of many debates. In our calculation, the two excitonic absorption bands (10 K) assigned to the special pair of *Rps. viridis*: 990 nm for P$_-$ and 850 nm for P$_+$, have been resolved using linear dichrism by Breton and co-workers,[42,44] and later the assignments of the bands were corroborated by Schulten and co-workers.[77] At room temperature, an analysis of the absorption spectrum of *Rps. viridis* by Michel and co-workers concludes that P$_-$ lies at 964 nm whereas P$_+$ lies near 811 nm.[103] Previous theoretical analysis of the absorption and CD spectra of *Rps. viridis* at 77 K assigns the majority of P$_+$ to 811 nm, in addition to sandwiching the exciton states B$_-$ (at 838 nm) and B$_+$ (at 830 nm) between P$_+$ (811 nm) and P$_-$ (964 nm),[103] which is in disagreement with linear dichroism measurements.[44] Thus, we agree with the conclusion of Schulten and co-workers[77] that any successful exciton model for the RC *Rps. viridis* must attribute a large fraction of the intensity at 850 nm to P$_+$, rather than to the accessory BChl$_b$ transitions.

For the *Rps. viridis* RC at 298 K, the calculated EET times from the results section were used to simulate the population kinetics of B and P$_-$. The B population decays with a single-exponential time constant of 215 fs, whereas the P$_-$ population rises with a 239 fs time constant (after assuming $(k_{ic})^{-1} = 50$ fs). By fitting the decay of the population of H, a time constant of 175 fs is obtained. The only report on EET in *Rps. viridis* RC at 298 K we found in the literature gives a P$_-$ bleach that appears within $\approx$90 fs after excitation of B, and within $\approx$170 fs after excitation of H.[16] Although the trends in the calculated H decay time and P$_-$ rise time agree with the experimental results, the agreement between our results and the experimental EET times is inferior to that for our *Rb. sphaeroides* calculations. The decay in the population of B in *Rps. viridis* is also predicted to be fairly temperature independent: at 200 K it is 208 fs, at 100 K it is 199 fs, and at 10 K it is 192 fs. Vos et al. measured the EET time from B to P$_+$ at 298 K to be $\approx$ 90 fs and at 10 K to be $\approx$ 80 fs.[16] However, in *Rps viridis*, the calculated rise times are approximately 2.5 times slower than the experimental values. Again, refer to Table 5 for a comparison between time constants extracted from fitting the population kinetics with our calculated EET times and the experimental population dynamics in the RC.

To understand the error in the calculated EET times in *Rps. viridis* we compare and contrast them with the *Rb. sphaeroides* results. The experimental P$_-$ rise times are approximately twice as fast in *Rps. viridis* than in *Rb. sphaeroides*. The arrangement of the cofactors is very similar in both species;[2,104,105] however, at both 298 and 10 K, the energy difference between the P$_-$ absorption band and the B fluorescence is $\approx$ 700 cm$^{-1}$ greater in *Rps. viridis* than in *Rb. sphaeroides*. As a consequence, the spectral overlap (at 10 K) between the B DOS and the P$_-$ DOS is $\approx$ 50% less in *Rps. viridis* than in *Rb. sphaeroides*. Even though the B to P$_-$ pathway has a much smaller contribution to the overall rate, the reduced spectral overlap with P$_-$ can

explain the $\approx$ 20% slower rise time of the population of P$_-$ in *Rps. viridis* at room temperature. The remainder of the discrepancy between the experiments and our calculation results for *Rps. viridis* may arise from the pairwise electronic couplings.

**F. Mutant Reaction Centers from *Rb. sphaeroides*.** Table 5 shows a comparison of our calculated results with the experimental data for the two RC mutants (beta and heterodimer) that we have investigated. The adequate agreement between the experiments and our EET calculations on various mutant reaction centers suggests that our generalized version of Förster theory should be applicable to a variety of aggregate systems.[24,106]

To compare our calculations with the fluorescence rise and decay of P in the beta mutant measured by Boxer and co-workers[13] we use the same method employed in section C for H to P EET, i.e. ($\beta_L$ or H$_M$) $\rightarrow$ B $\rightarrow$ P$_+$ $\rightarrow$ P$_-$ $\xrightarrow{k_{CS}}$ P$^+$H$^-$ with the four calculated EET rates from H (or $\beta$) to B, the four calculated EET rates from B to P, and the experimental[78] $(k_{CS})^{-1}$ = 3.3 ps at 77 K. When the initial state is $\beta_L$, the rise of the calculated kinetics of P$_-$ is best fit with a monoexponential rise of 250 fs. However, when the initial state is H$_M$ the calculated kinetics of P$_-$ are best fit to a rise of 480 fs. Fluorescence up-conversion measurements at 85 K report rise times of P$_-$ of 239 $\pm$ 35 fs for $\beta_L$ to P, 300 fs $\pm$ 11fs for H$_M$ to P, and 162 $\pm$ 25 fs for B to P.[13] Thus, our calculated results have modest agreement with the experimental finding of somewhat slower EET along the M branch of the beta mutant than on the L branch.

In the heterodimer, the calculated EET time at 77 K from B$_M$ to D is 278 fs and from B$_L$ to D is 710 fs. Our result agrees with experimental findings at 85 K, which measure the biexponential rise of the fluorescence from D to be 784 fs (amplitude 1.15) and 139 fs (amplitude 1.0) when excited at 795 nm (B$_L$), and 873 fs (amplitude 0.53) and 99 fs (amplitude 1.0) when excited at 807 nm (B$_M$).[17]

In the beta mutant, the pigment that is mutated from H$_L$ to bacteriochlorophyll, $\beta_L$, has highly localized excitations, and we scaled the coupling to it by the amount dictated by the dipole approximation. The change in the couplings produced by this mutation does not have significant influence on the dynamics. The important consequence of replacing a BPhe$_a$ with a BChl$_a$ in the H$_L$ binding is a change of spectral overlap originating from the site energy differences. The spectral overlap between the $\beta_L$ DOS and the B$_L$ DOS is increased over the wild-type value by 60%; and in turn, the calculated overall H to B transfer time at 77 K is 140 fs faster in the beta mutant than in the wild-type.

The situation in the heterodimer is quite different than in the beta mutant because the pigment that is mutated, P$_M$ to H, is part of the strongly coupled special pair acceptor. As in the special pair of the wild-type, the dipole approximation fails at the pairwise level, and $V_{D_L-D_M}$ must be modified to match the CD and absorption spectra. If the electronic couplings between the mutated pigment and all others are merely reduced by the amount expected from the dipole approximation, i.e., 12%, the calculated EET times do not match the experimental results. Because the pairwise electronic couplings have not been calculated for the heterodimer mutant, we follow the suggestion of Hammes et al.,[86] which corresponds to a 50% reduction in the electronic coupling within D. We infer that this reduction extends to the coupling between D$_M$ and the other pigments of the RC. It is not surprising that the couplings to D$_M$ need to be halved since the specific interactions with the Mg of the coordinating His ligand can affect the transition densities, site

Bacterial Photosynthetic Reaction Center

*J. Phys. Chem. B, Vol. 105, No. 8, 2001* **1667**

energies, and oscillator strengths in a manner not obvious from the dipole approximation. This reduction of the coupling may also be attributed to reorientation of the pigments or the mixing of charge transfer states, but we cannot specify the origin of this reduced coupling at present.

To understand the physical origin of the biexponential rate from B to D in the heterodimer,[17] one must first look at the electronic couplings in the wild-type (refer to Table 2). Because of the orientation factor between transition dipole moments of $P_M$ and $B_M$, the coupling on the M side of the special pair is largest with the L side donor pigments, e.g., $V(P_M-B_L) = -104$ cm$^{-1}$, but $V(P_M-B_M) = -16$ cm$^{-1}$. By replacing BChl$_a$ with a BPhe$_a$ in the $P_M$ binding site ($P_M$ to $D_M$), we reduce the coupling between the $D_M$ and all pigments by 50%, which results in $V(D_M-B_L) = -52$ cm$^{-1}$ and $V(D_M-B_M) = -8$ cm$^{-1}$. Recall that in the wild-type the EET time from $B_L$ to P is major contribution in the overall B to P rate. Thus, the reduction of the coupling between $D_M$ and the L side pigments affects the fastest pathway. Hence, based on the electronic coupling factors, the EET time will be slower along the L branch but resemble the wild-type along the M branch. This is evident in the four possible EET pathways from B to D by looking at $|V_{\delta\alpha}|^2 J_{\delta\alpha}(\epsilon)$ as shown in the lower panel of Figure 13. When a sum over two acceptor D states is taken, e.g., $B_M/D_L + B_M/D_M$, so as to model the EET time along each branch, the integrated area of $B_M/D$ is 3.5 times larger than the area of $B_L/D$ at 298 K and 2.6 times larger at 77 K.

Therefore, our calculations suggest that the electronic energy transfer from B to D in the heterodimer proceeds via a different pathway than in the wild-type. Despite the greater spectral overlap between either $B_M$ or $B_L$ and $D_M$ (see upper panel of Figure 13), the electronic coupling is largest between $B_M$ and $D_L$. Summation over the $|V_{\delta\alpha}|^2 J_{\delta\alpha}(\epsilon)$ (lower panel of Figure 13) of the two donor states, e.g., $B_M/D_M + B_L/D_M$, to determine the average B to D EET times reveals that of the four $\int d\epsilon$ $|V_{\delta\alpha}|^2 J_{\delta\alpha}(\epsilon)$ values, the integrated area of $B/D_L$ is 65% larger than that of $B/D_M$. The significant area in the region of 900 nm in the $|V_{\delta\alpha}|^2 J_{\delta\alpha}(\epsilon)$ is specific to the heterodimer. Contrary to the wild-type pathway in which most of the energy flows to $P_+$, here energy flows to the exciton state having the largest composition of $D_L$, i.e., the lowest energy state.

## VI. Model Limitations and Assumptions

In this section we describe possible limitations to our energy transfer model and specify some assumptions employed in calculating the EET dynamics in the RC. It has been suggested by several authors that a configuration interaction between locally excited (e.g., B*P and BP*) and charge transfer (e.g., B$^+$P$^-$ and B$^-$P$^+$) states is of possible significance in mediating this coupling.[37,107,108] If such terms were significant, one would have to go beyond our model for the pairwise couplings in order to include those contributions which depend on orbital overlap. This should be a small correction and would not affect our conclusions. If the charge transfer states are low-lying at the ground-state equilibrium reaction coordinate, then explicit inclusion of charge transfer states in the model may reveal different types of dynamics. For example, it has been suggested that after excitation of B or H, direct charge separation (P$^+$B$_L^-$, P$^+$H$_L^-$, or B$^+$H$_L^-$) occurs in the wild-type RC from *Rb. sphaeroides* at 77 K[109] and at 15 K.[16] Van Brederode et al. postulated that the formation of P$^+$B$_L^-$, which must occur in $\approx$ 200 fs, competes with EET from B to P.[109] Due to the large difference in rates between the wild-type and heterodimer,

charge separation from B could more effectively compete with EET in the heterodimer.

In this work we have assumed that the line shapes (bandwidths and vibronic progressions) for the P$_-$ and P$_+$ transitions are identical, and find that with this assumption we can reproduce the experimental absorption and circular dichroism spectra satisfactorily. Our approach limits the number of adjustable parameters and is consistent with the spectral line shapes used by Won and Friesner at 5 K. However, we note that linear dichroism data has revealed different line widths for the two special pair exciton states. In this regard, a calculation of the linear dichroism spectrum to extract the true P$_+$ line shape could prove to be useful. Even so, we do not expect a narrower line shape for P$_+$ to alter the spectral overlap enough to change our understanding of EET in the RC. This change should be even smaller than the small affect that the Stokes shift of B has on the EET dynamics as discussed previously.

We have not explicitly estimated the errors in our calculations because of the large number of parameters that derive from various sources. Our calculations capture the essential physical picture of how energy is transferred in the RC, but we do not expect perfect quantitative agreement between the calculated and experimental values. The largest source of error most likely originates from the pairwise electronic couplings. As previously mentioned, the electronic couplings between the pigments are assumed to be identical in both RC species *Rb. sphaeroides* and *Rps. viridis*. Also, the couplings used in the EET calculation of all the RC species are calculated from the *Rps. viridis* crystal structure using the dipole approximation. The transition moment orientations as revealed by crystallographic studies are very similar for *Rps. viridis* and *Rb. sphaeroides*,[2,104,105] although it is possible that the oscillator strength of BChl$_b$ in *Rps. viridis*[109] might be different than BChl$_a$ in *Rb. sphaeroides*.[111,112] Our calculation of EET in *Rps. viridis* predicts two times slower EET rates than the experimental values. This observation is consistent with the values of $V_{mn}$ in Table 2 and suggests that the true electronic interactions in *Rps. viridis* may be underestimated.

In the present study, the electronic coupling between sites is obtained by interacting transition dipoles associated with molecular centers of the donors and acceptors (Figure 3b of the accompanying paper), rather then assuming that transition dipoles are associated with donor and acceptor supermolecules (Figure 3c of the accompanying paper). However, to improve our estimates of the pairwise electronic couplings (aside from $P_L-P_M$) from the distributed transition dipoles used here, we could undertake transition density cube (TDC) calculations. An advantage of such calculations is that dielectric screening effects could be determined simultaneously. However, by performing the present study using the dipole–dipole pairwise couplings we have been able to ascertain that this is a reasonable approximation *provided that we correctly calculate $V_{\delta\alpha}$ and the associated spectral overlaps*. This is an important conclusion because the available structural information is not always detailed enough to justify the undertaking of large quantum chemical calculations to determine accurate electronic couplings between each pair of molecules in the aggregate.

## VII. Concluding Remarks

In this work, we have attempted to answer the following questions concerning energy transfer in the bacterial reaction center. (1) Are the dynamics promoted by a weak-coupling or strong-coupling mechanism? (2) Is the mechanism of energy transfer from H to P qualitatively different from B to P because

of the nature of the intermediate B? (3) Given that the special pair is a strongly coupled dimer, what is the principal acceptor state? (4) How can we rationalize the temperature independence of energy transfer in the RC? (5) Do the vibrational motions of the special pair play a mechanistic role in energy transfer? (6) Is the mechanism of EET in a variety of mutants different or the same as that in the *Rb. sphaeroides* wild-type?

Our work provides the following answers: (1) The EET dynamics in the RC are promoted via a weak-coupling mechanism. Most importantly, we had to adapt Förster theory so that it could be applied to molecular aggregates such as the RC. Our model employed only Coulombic couplings (aside from the coupling within the special pair), and we conclude that short-range interactions, depending explicitly on orbital overlap between the pigments are relatively unimportant. Crucially, we had to calculate correctly the *effective* donor−acceptor couplings and their associated spectral overlaps. Simple application of Förster theory blurs the details of the aggregate and leads to physically incorrect results. (2) Our calculated results indicate that energy is transferred according to the following scheme H → B → P$_+$(→P$_-$) and can be modeled with this generalized version of Förster theory. In addition, the calculated decay and rise times for B and P$_-$ in this scheme are in satisfactory agreement with experimental results. (3) Our calculations suggest that P$_+$ is the principal acceptor state involved in energy transfer from B to P in the wild-type RC. (4) The temperature independence of EET can be understood via the spectral overlap between B and P$_+$ densities of states. This overlap governs the rate, and we have found it to be insensitive to temperature. The overlap between the B and P$_-$ densities of states, since P$_-$ peaks at 865 nm at 298 K and at 890 nm at 10 K, is affected by temperature, but is relatively unimportant in the overall dynamic process. (5) The large displacements of the vibrational modes of P make an important contribution to the EET by increasing the spectral overlap between B and P$_+$, which in turn increases the rate and plays a role in the temperature independence. (6) The same weak-coupling mechanism, i.e., the generalized Förster theory presented here, provides an adequate description of EET in both the beta and heterodimer mutants, although in the case of the heterodimer, the calculations depend on an assumption of decreased electronic coupling between D$_M$ and the rest of the RC pigments. In the beta mutant, where the weakly coupled H$_M$ chromophore is replaced with a BChl$_a$, energy transfer is both quantitatively and mechanistically similar to the wild-type. However, in the heterodimer mutant, where the mutated pigment is part of a strongly coupled special pair, the energy transfer proceeds at a quite different rate along each branch. This leads to a biexponential rise of population of the P state.

**Supporting Information Available:** Table IS: the vibrational frequencies, $\omega$, and Huang−Rhys factors, $S$, for P, B and H used to calculate the line shape functions. Table IIS: $\omega$ and $S$ used for P below 100 K. Table IIIS: our calculated temperature dependence of the B to P EET times in the RC. This information is available free of charge via the Internet at http://pubs.acs.org.

**References and Notes**

(1) Chang, C. H.; Elkabbani, O.; Tiede, D.; Norris, J.; Schiffer, M. *Biochemistry* **1991**, *30*, 5352.
(2) Norris, J. R.; Budil, D. E.; Gast, P.; Chang, C. H.; Elkabbani, O.; Schiffer, M. *Proc. Natl. Acad. Sci. U.S.A.* **1989**, *86*, 4335.
(3) Hoff, A. J.; Deisenhofer, J. *Phys. Rep. (Netherlands)* **1997**, *287*, 1.
(4) Michel, H. *J. Mol. Biol.* **1982**, *158*, 567.
(5) Deisenhofer, J.; Epp, O.; Sinning, I.; Michel, H. *J. Mol. Biol.* **1995**, *246*, 429.
(6) Ermler, U.; Fritzsch, G.; Buchanan, S. K.; Michel, H. *Structure* **1994**, *2*, 925.
(7) Slooten, L. *Biophys. Biochim. Acta* **1972**, *256*, 452.
(8) Breton, J.; Martin, J.-L.; Migus, A.; Antonetti, A.; Orszag, A. *Proc. Natl. Acad. Sci. U.S.A.* **1986**, *83*, 5121.
(9) Breton, J.; Martin, J.-L.; Fleming, G. R.; Lambry, J.-C. *Biochemistry* **1988**, *27*, 8276.
(10) Jia, Y. W.; Jonas, D. M.; Joo, T. H.; Nagasawa, Y.; Lang, M. J.; Fleming, G. R. *J. Phys. Chem.* **1995**, *99*, 6263.
(11) Jonas, D. M.; Lang, M. J.; Nagasawa, Y.; Bradforth, S. E.; Dikshit, S. N.; Jimeniz, R.; Joo, T.; Fleming, G. R. In *Proceedings of the Feldafing III Workshop*; Munich, 1995.
(12) Jonas, D. M.; Lang, M. J.; Nagasawa, Y.; Joo, T.; Fleming, G. R. *J. Phys. Chem.* **1996**, *100*, 12660.
(13) Stanley, R. J.; King, B.; Boxer, S. G. *J. Phys. Chem.* **1996**, *100*, 12052.
(14) Lin, S.; Taguchi, A. K. W.; Woodbury, N. W. *J. Phys. Chem.* **1996**, *100*, 17067.
(15) Haran, G.; Wynne, K.; Moser, C. C.; Dutton, P. L.; Hochstrasser, R. M. *J. Phys. Chem.* **1996**, *100*, 5562.
(16) Vos, M. H.; Breton, J.; Martin, J. L. *J. Phys. Chem. B* **1997**, *101*, 9820.
(17) King, B. A.; Stanley, R. J.; Boxer, S. G. *J. Phys. Chem. B* **1997**, *101*, 3644.
(18) Vulto, S. I. E.; Streltsov, A. M.; Shkuropatov, A. Y.; Shuvalov, V. A.; Aartsma, T. J. *J. Phys. Chem. B* **1997**, *101*, 7249.
(19) Arnett, D. C.; Moser, C. C.; Dutton, P. L.; Scherer, N. F. *J. Phys. Chem. B* **1999**, *103*, 2014.
(20) King, B. A.; McAnaney, T.; deWinter, A.; Boxer, S. G. *J. Phys. Chem. B* **2000**, *104*, 8895.
(21) Jean, J. M.; Chan, C.-K.; Fleming, G. R. *Isr. J. Chem.* **1988**, *28*, 169.
(22) Johnson, S. G.; Tang, D.; Jankowiak, R.; Hayes, J. M.; Small, G. J.; Tiede, D. M. *J. Phys. Chem.* **1990**, *94*, 5849.
(23) Sumi, H. *J. Phys. Chem. B* **1999**, *103*, 252.
(24) Scholes, G. D.; Fleming, G. R. *J. Phys. Chem. B* **2000**, *104*, 1854.
(25) Warshel, A.; Parson, W. W. *J. Am. Chem. Soc.* **1987**, *109*, 6152.
(26) Warshel, A.; Parson, W. W. *J. Am. Chem. Soc.* **1987**, *109*, 6143.
(27) Friesner, R. A.; Won, Y. D. *J. Phys. Chem.* **1988**, *92*, 2208.
(28) Friesner, R. A.; Won, Y. D. *J. Phys. Chem.* **1988**, *92*, 2214.
(29) Won, Y.; Friesner, R. A. In *The Photosynthetic Bacterial Reaction Center: Structure and Dynamics*; Breton, J., Vermeglio, A., Eds.; Plenum Press: New York, 1988; Vol. I, p 341.
(30) Friesner, R. A.; Won, Y. D. *Biophys. Biochim. Acta* **1989**, *977*, 99.
(31) Lathrop, E. J. P.; Friesner, R. A. *J. Phys. Chem.* **1994**, *98*, 3056.
(32) Thompson, M. A.; Zerner, M. C. *J. Am. Chem. Soc.* **1991**, *113*, 8210.
(33) Thompson, M. A.; Zerner, M. C.; Fajer, J. *J. Phys. Chem.* **1991**, *95*, 5693.
(34) Knapp, E. W.; Scherer, P. O. J.; Fischer, S. F. *Biophys. Biochim. Acta* **1986**, *852*, 295.
(35) Scherer, P. O. J.; Fischer, S. F. *Chem. Phys. Lett.* **1986**, *131*, 153.
(36) Scherer, P. O. J.; Fischer, S. F. *Biophys. Biochim. Acta* **1987**, *891*, 157.
(37) Scherer, P. O. J.; Fischer, S. F. *Chem. Phys.* **1989**, *131*, 115.
(38) Hasegawa, J.; Ohkawa, K.; Nakatsuji, H. *J. Phys. Chem. B* **1998**, *102*, 10410.
(39) Nakatsuji, H.; Hasegawa, J.; Ohkawa, K. *Chem. Phys. Lett.* **1998**, *296*, 499.
(40) Scholes, G. D.; Jordanides, X. J.; Fleming, G. R. *J. Phys. Chem. B* **2001**, *105*, 1640.
(41) Scherer, P. O. J.; Fischer, S. F.; Horber, J. K. H.; Michel-Beyerle, M. E.; Michel, H. In *Antennas and Reaction Centers of Photosynthetic Bacteria: Structure, Interactions, and Dynamics*; Feldafind: Bavaria, 1985.
(42) Breton, J. In *The Photosynthetic Bacterial Reaction Center: Structure and Dynamics*; Breton, J., Vermeglio, A., Eds.; Plenum Press: New York, 1988; Vol. I.; p 59.
(43) Hartwich, G.; Scheer, H.; Aust, V.; Angerhofer, A. *Biochim. Biophys. Acta* **1995**, *1230*, 97.
(44) Breton, J. *Biochim. Biophys. Acta* **1985**, *810*, 235.
(45) Kirmaier, C.; Gaul, D.; Debey, R.; Holten, D.; Schenck, C. C. *Science* **1991**, *251*, 922.

Bacterial Photosynthetic Reaction Center

*J. Phys. Chem. B, Vol. 105, No. 8, 2001* **1669**

(46) Steffen, M. A.; Lao, K. Q.; Boxer, S. G. *Science* **1994**, *264*, 810.

(47) Spiro, T. G. *Resonance Raman Spectra of Polyenes and Aromatics*; Wiley: New York, 1987.

(48) Lee, S.-Y.; Heller, E. J. *J. Chem. Phys.* **1979**, *71*, 4777.

(49) Myers, A. B. *J. Opt. Soc. Am. B* **1990**, *7*, 1665.

(50) Myers, A. B. *Chem. Phys.* **1994**, *180*, 215.

(51) Myers, A. B. *J. Raman Spectrosc.* **1997**, *28*, 389.

(52) Shreve, A. P.; Cherepy, N. J.; Franzen, S.; Boxer, S. G.; Mathies, R. A. *Proc. Natl. Acad. Sci. U.S.A.* **1991**, *88*, 11207.

(53) Cherepy, N. J.; Shreve, A. P.; Moore, L. J.; Franzen, S.; Boxer, S. G.; Mathies, R. A. *J. Phys. Chem.* **1994**, *98*, 6023.

(54) Cherepy, N. J.; Shreve, A. P.; Moore, L. J.; Boxer, S. G.; Mathies, R. A. *Biochemistry* **1997**, *36*, 8559.

(55) Cherepy, N. J. Electronic and Nuclear Dynamics of the Bacterial Photosynthetic Reaction Center and Chorosomes from Resonance Raman Intensities. Ph.D Thesis, University of California, Berkeley, 1996.

(56) Palaniappan, V.; Martin, P. C.; Chynwat, V.; Frank, H. A.; Bocian, D. F. *J. Am. Chem. Soc.* **1993**, *115*, 12035.

(57) Vos, M. H.; Rappaport, F.; Lambry, J. C.; Breton, J.; Martin, J. L. *Nature* **1993**, *363*, 320.

(58) Vos, M. H.; Jones, M. R.; Martin, J. L. *Chem. Phys.* **1998**, *233*, 179.

(59) Stanley, R. J.; Boxer, S. G. *J. Phys. Chem.* **1995**, *99*, 859.

(60) Cherepy, N. J.; Shreve, A. P.; Moore, L. J.; Boxer, S. G.; Mathies, R. A. *J. Phys. Chem. B* **1997**, *101*, 3250.

(61) Gillie, J. K.; Small, G. J.; Golbeck, J. H. *J. Phys. Chem.* **1989**, *93*, 1620.

(62) Fleming, G. R.; Passino, S. A.; Nagasawa, Y. *Philos. Trans. R. Soc. (London) A* **1998**, *356*, 389.

(63) Jordanides, X. J.; Lang, M. J.; Song, X. Y.; Fleming, G. R. *J. Phys. Chem. B* **1999**, *103*, 7995.

(64) Mukamel, S. *Principles of Nonlinear Optical Spectroscopy*; Oxford University Press: New York, 1995.

(65) Meech, S. R.; Hoff, A. J.; Wiersma, D. A. *Proc. Natl. Acad. Sci. U.S.A.* **1986**, *83*, 9464.

(66) Johnson, S. G.; Tang, D.; Jankowiak, R.; Hayes, J. M.; Small, G. J.; Tiede, D. M. *J. Phys. Chem.* **1989**, *93*, 5953.

(67) Middendorf, T. R.; Mazzola, L. T.; Gaul, D. F.; Schenck, C. C.; Boxer, S. G. *J. Phys. Chem.* **1991**, *95*, 10142.

(68) Reddy, N. R. S.; Lyle, P. A.; Small, G. J. *Photosynth. Res.* **1992**, *31*, 167.

(69) Lyle, P. A.; Kolaczkowski, S. V.; Small, G. J. *J. Phys. Chem.* **1993**, *97*, 6924.

(70) Groot, M. L.; Yu, J. Y.; Agarwal, R.; Norris, J. R.; Fleming, G. R. *J. Phys. Chem. B* **1998**, *102*, 5923.

(71) Yu, J. Y.; Nagasawa, Y.; vanGrondelle, R.; Fleming, G. R. *Chem. Phys. Lett.* **1997**, *280*, 404.

(72) Jimenez, R.; vanMourik, F.; Yu, J. Y.; Fleming, G. R. *J. Phys. Chem. B* **1997**, *101*, 7350.

(73) Wiersma, D. In *The Photosynthetic Bacterial Reaction Center: Structure and Dynamics*; Breton, J., Vermeglio, A., Eds.; Plenum Press: New York, 1988; Vol. I.; p 351.

(74) Fidder, H.; Knoester, J.; Wiersma, D. A. *J. Chem. Phys.* **1991**, *95*, 7880.

(75) King, B. A. Personal communication.

(76) Förster, T. *Ann. Phys.* **1948**, *2*, 55.

(77) Eccles, J.; Honig, B.; Schulten, K. *Biophys. J.* **1988**, *53*, 137.

(78) Kirmaier, C.; Laporte, L.; Schenck, C. C.; Holten, D. *J. Phys. Chem.* **1995**, *99*, 8910.

(79) Connolly, J. S.; Samuel, E. B.; Janzen, F. E. *Photochem. Photobiol.* **1982**, *36*, 565.

(80) The 20−30% increase in the oscillator strength is proportional to the increase in dipole strength. Since the ratio of the dipole strengths $\mu_B^2/\mu_H^2 = 1.20-1.30$, the transition dipole moment ratio $\mu_B/\mu_H = 1.1-1.14$. This corresponds to 10−14% increase in the electronic couplings.

(81) Chirino, A. J.; Lous, E. J.; Huber, M.; Allen, J. P.; Schenck, C. C.; Paddock, M. L.; Feher, G.; Rees, D. C. *Biochemistry* **1994**, *33*, 4584.

(82) Palaniappan, V.; Schenck, C. C.; Bocian, D. F. *J. Phys. Chem.* **1995**, *99*, 17049.

(83) Bylina, E. J.; Youvan, D. C. *Proc. Natl. Acad. Sci. U.S.A.* **1988**, *85*, 7226.

(84) Kirmaier, C.; Holten, D.; Bylina, E. J.; Youvan, D. C. *Proc. Natl. Acad. Sci. U.S.A.* **1988**, *85*, 7562.

(85) Breton, J.; Bylina, E. J.; Youvan, D. C. *Biochemistry* **1989**, *28*, 6423.

(86) Hammes, S. L.; Mazzola, L.; Boxer, S. G.; Gaul, D. F.; Schenck, C. C. *Proc. Natl. Acad. Sci. U.S.A.* **1990**, *87*, 5682.

(87) Zhou, H. L.; Boxer, S. G. *J. Phys. Chem. B* **1997**, *101*, 5759.

(88) Beekman, L. M. P.; van Stokkum, I. H. M.; Monshouwer, R.; Rijnders, A. J.; McGlynn, P.; Visschers, R. W.; Jones, M. R.; van Grondelle, R. *J. Phys. Chem.* **1996**, *100*, 7256.

(89) Sauer, K. H. Personal communication.

(90) Beese, D.; Steiner, R.; Angerhofer, A.; Robert, B.; Lutz, M. *Photochem. Photobiol.* **1988**, *47*, 293.

(91) Tinoco, I., Jr. *Adv. Chem. Phys.* **1962**, *4*, 113.

(92) Mar, T.; Gingras, G. *Biochemistry* **1995**, *34*, 9071.

(93) This assumption is consistent with the kinetic analyses of the experimental data of Martin and co-workers[16] and Scherer and co-workers.[19] The former obtain energy transfer times of ∼200 fs from B to P$_+$ and 50−100 fs from B to P$_−$, while the latter obtain EET times of ∼120 fs from B to P$_+$ and ∼ 65 fs from P$_+$ to P$_−$. On the other hand, this assumption is inconsistent with the earlier kinetic analysis of our group,[12] which estimates that EET from B to P$_+$ occurs in ∼ 80 fs and internal conversion occurs in ∼ 150 fs.

(94) Kuki, A. *Struct. Bonding* **1991**, *75*, 49.

(95) Jordan, K. D.; Paddon-Row: M. N. *Chem. Rev.* **1992**, *92*, 395.

(96) Curtiss, L. A.; Naleway, C. A.; Miller, J. R. *J. Phys. Chem.* **1993**, *97*, 4050.

(97) Shephard, M. J.; Paddon-Row: M. N. *J. Phys. Chem.* **1995**, *99*, 17497.

(98) This is often not satisfied. Figure 8 of the accompanying paper shows the lack of correlation between the electronic coupling of B800 to B850 and the corresponding dipole strength of each B850 eigenstate.

(99) Scholes, G. D.; Gould, I. R.; Cogdell, R. J.; Fleming, G. R. *J. Phys. Chem. B* **1999**, *103*, 2543.

(100) Choi, S. I.; Jortner, J.; Rice, S. A.; R.; S. *J. Chem. Phys.* **1964**, *41*, 3294.

(101) Harcourt, R. D.; Scholes, G. D.; Ghiggino, K. P. *J. Chem. Phys.* **1994**, *101*, 10521.

(102) $V_{mn}$ of eq 11 in the accompanying paper never equals the coupling within the special pair. In addition, the coefficients $\lambda_{\delta,m}$ and $\lambda_{a,n}$ of eq 11 in the companion paper[40] do not change as a function of temperature for $\delta$ = B and $\alpha$ = P.

(103) Knapp, E. W.; Fischer, S. F.; Zinth, W.; Sander, M.; Kaiser, W.; Deisenhofer, J.; Michel, H. *Proc. Natl. Acad. Sci. U.S.A.* **1985**, *82*, 8463.

(104) Feher, G.; Allen, J. P.; Okamura, M. Y.; Rees, D. C. *Nature* **1989**, *339*, 111.

(105) Lancaster, C. R. D.; Michel, H. *Photosynth. Res.* **1996**, *48*, 65.

(106) Walla, P. J.; Linden, P. A.; Hsu, C. P.; Scholes, G. D.; Fleming, G. R. *Proc. Natl. Acad. Sci. U.S.A.* **2000**, *97*, 10808.

(107) Warshel, A.; Creighton, S.; Parson, W. W. *J. Phys. Chem.* **1988**, *92*, 2696.

(108) Zhang, L. Y.; Friesner, R. A. *Proc. Natl. Acad. Sci. U.S.A.* **1998**, *95*, 13603.

(109) Van Brederode, M. E.; van Mourik, F.; van Stokkum, I. H. M.; Jones, M. R.; van Grondelle, R. *Proc. Natl. Acad. Sci. U.S.A.* **1999**, *96*, 2054.

(110) Shuvalov, V. A.; Asadov, A. A. *Biophys. Biochim. Acta* **1979**, *545*, 653.

(111) Scherz, A.; Parson, W. W. *Biophys. Biochim. Acta* **1984**, *766*, 296.

(112) Connolly, J. S.; Samuel, E. B.; Janzen, A. F. *Photochem. Photobiol.* **1982**, *36*, 565.